NATURAL DYE SENSITIZED PHOTHOELECTROCHEMICAL CELLS BASED ON ZINC OXIDE NANOPARTICLES

Getachew Yirga

A THESIS SUBMITTED TO MATERIALS SCIENCE PROGRAM

PRESENTED IN PARTIAL FULFILLMENT OF THE REQUIREMENTS

FOR THE DEGREE OF MASTER OF SCIENCE (MATERIALS SCIENCE)

ADDIS ABABA UNIVERSITY

ADDIS ABABA, ETHIOPIA

ADDIS ABABA UNIVERSITY

SCHOOL OF GRADUATE STUDY

Date: JUNE:2012

Author:	Getachew Yirga Solomon
Title:	Natural dye senistized photoelectrochemical cells Based on ZnO Nanoparticles
Program:	Materials Science
Degree:	Masters of Science
Convocation:	JUNE:2012

_____

Signature of author

I hereby declare that this thesis is my own work and effort and that it has not been submitted anywhere for any award. Where other sources of information have been used, they have been acknowledged.

ADDIS ABABA UNIVERSITY

SCHOOL OF GRADUATE STUDY

Date: JUNE:2012

This is to certify that the thesis prepared by **GETACHEW YIRGA** entitled: **NATURAL DYE SENSITIZED PHOTHOELECTROCHEMICAL CELLS BASED ON ZINC OXIDE NANOPARTICLES**, and submitted in partial fulfillment of the requirement of the degree of master of science compiles with the regulation of the University meet the accepted standards with respect to the originality and quality.

Signed by the examining committee:

Examiner	Prof. Javed Mazher	Signature _____	Date _____
Examiner	Dr. Tilak Bollepalli	Signature _____	Date _____
Advisor	Prof. Teketel Yohannes	Signature _____	Date _____
Chairman	Prof. Teketel Yohannes	Signature _____	Date _____

Abstract

Natural Dye Sensitized Phothoelectrochemical Cells Based On ZnO Nanoparticles.

Getachew Yirga

Addis Ababa University, 2012

This thesis focused on the study of dye-sensitized solar cells (DSSCs) based on ZnO nanoparticle. Our work started by synthesizing ZnO nanopartcile using sol-gel method. ZnO nanoparticles were synthesized and the size of the nanoparticle (1.14 nm) was determined by using effective mass approximation model.

Natural sensitizers extracted from *Jacaranda mimosifolia, Bougainvillea spectabilis, Carissa ovata, Amarathus iresine, Beta vulgaris, and Hibiscus sabdariffa* used for sensitizing ZnO nanoparticle. All natural sensitizers were extracted by water and ethanol, absorption spectra were measured and all natural sensitizers absorbs in the visible region. Devices were fabricated using ZnO nanoparticles and with all the above natural sensitizers, then the photoelectrochemical performance were measured. DSSCs based on ZnO nanoparticles and ethanol extract of *Amarathus iresine* sensitizers have shown relatively good conversion efficiency of 0.039.

The incident photon to current conversion efficiency (IPCE), short circuit current density (J_{sc}) and V_{oc} were measured for all the above sensitizers. Also comparative study were made using TiO_2 nanoparticle based DSSCs sensitized by *Bougainvillea Spectabilis, Carissa ovata, and Jacaranda mimosifolia* with ZnO based DSSCs sensitized by the same sensitizers. In TiO_2 nanopartcile based DSSCs the photoelectrochemical (PEC) performance we found relatively higher than the ZnO nanopartcles based DSSCs as expected. The data we got from TiO_2 and ZnO based DSSCs was analyzed and finally some of the problem that limit the conversion efficiency were discussed.

Acknowledgements

First of all, I would like to thank the almighty; God, for letting me to accomplish this work.

I am deeply indebted to Professor Teketel Yohannes, my advisor, for his support and friendly approach during this research. I also like to thank his PhD student Sisay Tadesse for his tireless follow up and his consistent support during my research work.

My strongest thank was goes to my family and my intimate friends, who lived for me. I would like to thank my host University Haramaya University for financial supporting during my stay, and Addis Ababa University specially Materials Science Program for letting me to study my postgraduate study. Finally I used derived materials from many research journals and books, and I am indebted to the authors of those publications and books.

Contents

List of Figures

List of Tables

Chapter 1

Introduction and motivation

Energy consumption is one of the most important aspects in people's everyday life. It exists in different forms, from burning woods to obtain fire in prehistoric times to electricity productions in modern age. However due to the rapid growth in industrialization in many countries the original sources of energy that people used to harvest have shown signs of deficiency. Therefore, people started searching for new resources for energy production. At the same time, people also realized the damages that the energy production has done to the environment. Therefore, researches have been increased rapidly to seek for clean and renewable energy resources that will power the future.

One of the most prominent clean and renewable energy is solar energy which has a great importance. Sun has always been the most powerful energy source on earth. It is clean, environmentally friendly and is for free. Sun provides approximately 100,000 terawatts to the Earth which is about 10,000 times more than the present rate of the worlds present energy consumption [1]. Photovoltaic cells and photoelectrochemical cells are devices that can transform the energy of the sunlight into useful form of energy. These two cells are being used increasingly to tap into this huge resource and will play a key role in future sustainable energy systems. So that if we successfully convert this energy into electricity our need of energy completely satisfied. Due to this reason so many researchers are focusing on this active research area.

1.1 History of photoelectrochemical cell

The photovoltaic effect was discovered by Alexandre-Edmond Becquerel, who was a French physicist. This was the beginning of the solar cell technology [2]. Becquerel's experiment was done by illuminating two electrodes with different types of light. The electrodes were coated by light sensitive materials, AgCl or AgBr, and carried out in a black box surrounded by an acid solution. The electricity increased when the light intensity increased. Willoughby Smith discovered the photovoltaic effect in selenium in 1873 [3]. In 1876, with his student R. E. Day, William G. Adams discovered that illuminating a junction between selenium and platinum also has a photovoltaic effect [4]. These two discoveries were the foundation for the first selenium solar cell construction, which was built in 1877 and later on Charles Fritts first described them in detail in 1883. It was later found that the photosensitivity can be extended to longer wavelengths by adding a dye to silver halide emulsions [5].

A photoelectrochemical cell is one type of photocurrent generated device which has a semiconductor in contact with an electrolyte. This cell consists of a photoactive semiconductor working electrode (either n or p-type) and counter electrode made of either metal (e.g. Pt) or semiconductors. Both electrodes are immersed in the electrolyte containing suitable redox couples. In a metal-electrolyte junction, the potential drop occurs entirely on the solution site, whereas in a semiconductor electrolyte junction, the potential drop occurs on the semiconductor site as well as the solution site. The charge on the semiconductor side were distributed deep in the interior of the semiconductor, creating a space charge region. If the junction of the semiconductor electrolyte is illuminated with a light having energy greater than the bandgap of the semiconductor, photogenerated electrons/holes are separated in the space charge region.

The photo-generated minority carriers arrive at the interface of the semiconductor electrolyte. Photo-generated majority carriers accumulate at the backside of the semiconductor. Then with the help of a connecting wire, photo-generated majority carriers are transported *via* a load to the counter electrode where these carriers electrochemically re-

act with the redox electrolyte.

The following are different types of photoelectrochemical cells with the working electrode (WE) made of semiconductor (n- or p-type) and the counter electrode (CE) platinum. When shining the light, oxidation reaction occur on the surface of n-type semiconductors, whilst reduction reaction will occur on the surface of p-type semiconductors. In the electrochemical photovoltaic cell, which is based on a narrow band gap semiconductor and a redox couple as shown in the Figure 1.1. Optical energy is converted into electrical energy without change of the free energy of the redox electrolyte ($\Delta G = 0$).

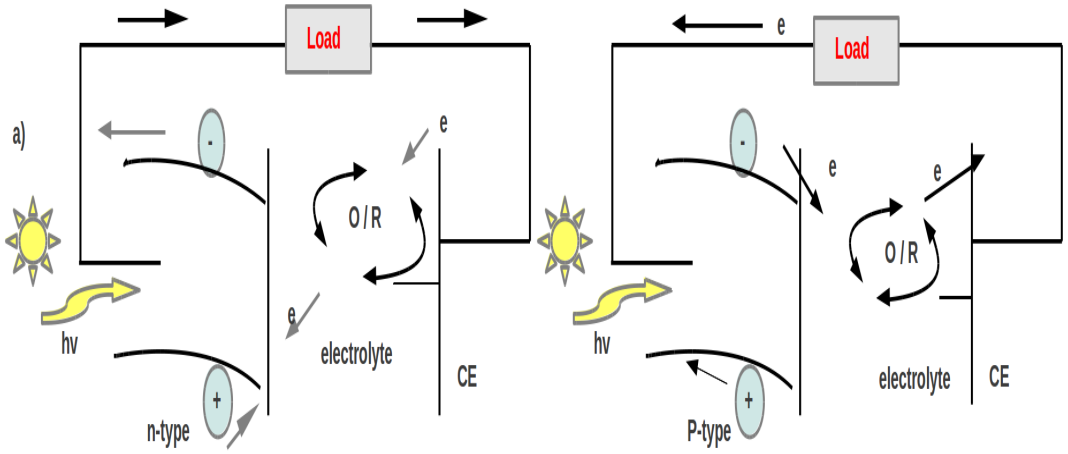

Figure 1.1: Electrochemical photovolatic cell.

The electrochemical reaction occurring at the counter electrode (CE) is opposite to the photo-assisted reaction occurring at the semiconductor working electrode. Thus, they are also called regenerative photoelectrochemical solar cells [6]. If the photogenerated energy is converted to chemical energy, the free energy of the electrolyte will have a change ($\Delta G \neq 0$).

Depending on the relative location of the potentials of the two redox couples (O/R and O'/R'), the photosynthetic cells containing two redox couples, can be further classified in to two cells. Photocatalytic cell ($\Delta G < 0$, Figure 1.2) where light merely serves to accelerate the reaction rate and photoelectrolytic cell ($\Delta G > 0$, Figure 1.3) where the cell reaction is driven by light [7].

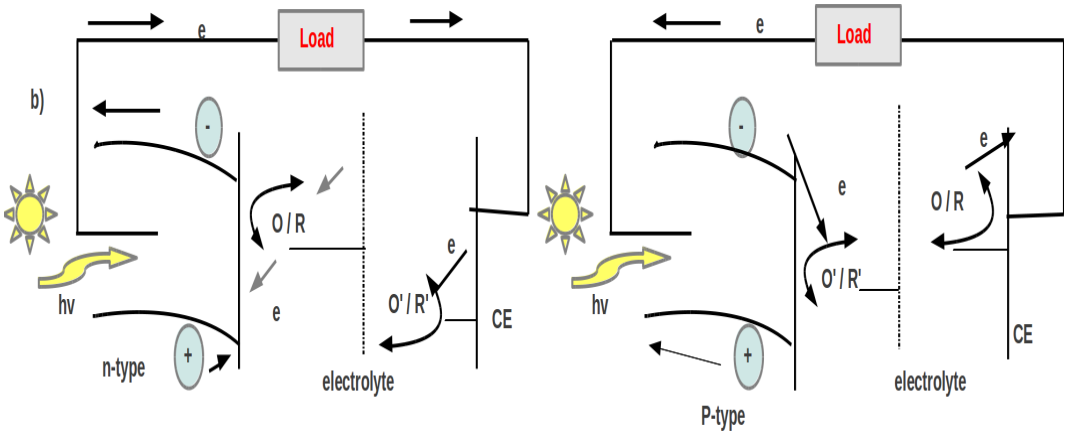

Figure 1.2: Electrochemical photocatalytic cell.

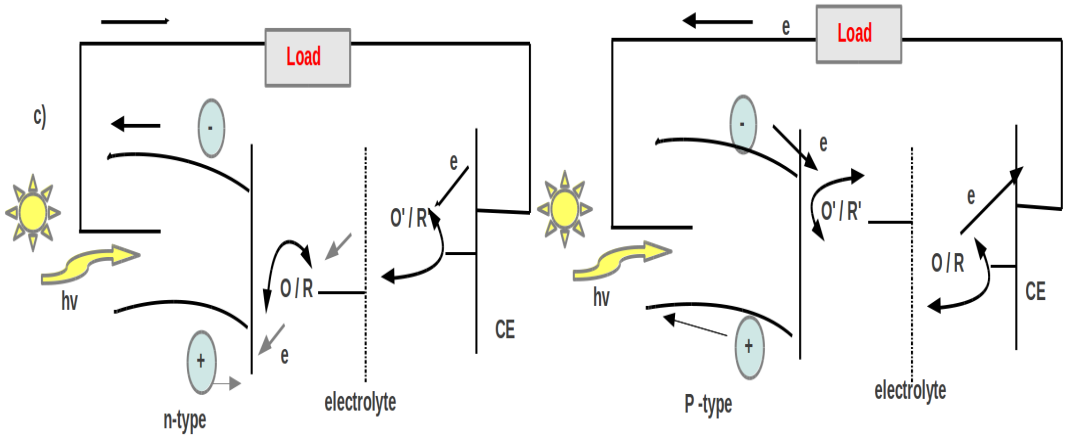

Figure 1.3: Electrochemical photoelectrolytic cell.

The type of molecular solar cell that this thesis focuses on appeared in the beginning of the 1990s. Brian Ò Regan and Michael Grätzel obtained about 10-11% efficiency with a new solar cell design, the nanoporous dye-sensitized solar cell (DSSC) [1]. The dye sensitized solar cell was a photo-electrochemical solar cell which use a liquid, quasi solid or solid electrolyte. The working electrode was made of nanoporous semiconductors covered with a monolayer of dye molecules. The dye molecules can be organic dyes or natural dyes which can be extracted from plants, fruits and flowers. More detailed explanation to natural dye sensitized photoelectrochemical cell is given in Chapter two.

1.2 Objective of the thesis

The general objective of the study is to construct and study photoelectrochemical cells based on natural dyes and zinc oxide nanoparticles.

Specific Objective

- Synthesis of ZnO nanoparticles using sol-gel method for using as a semiconductor in dye sensitized solar cell.
- Extraction of anthocyanins, chllorophyll, and betalains from *Jacaranda mimosifolia, Beta vulgaris, Bouganvillea, Amarathus iresine herbisiti, Hibiscus sabdariffa, and Carissa ovata*.
- Selecting natural sensitizers which have best absorption spectrum in the visible spectra of sunlight for using as natural sensitizers for ZnO semiconductor.

Chapter 2

Dye sensitized photoelectrochemical cell

Dye sensitized solar cell (DSSC) is one type of photoelectrochemical cell, which use a wide bandgap semiconductor as electrode for the cells due to their high photochemical stability. DSSCs work without the need for a built in electrical field, without a strict control of the purity of materials, and the presence of a huge internal interface is crucial for their good functioning.

The backbone of a DSSCs is a mesoporous layer of semiconductor oxide nanoparticles, which are sintered together to establish a good electric contact between the particles. The nanoparticle film is deposited on a glass plate covered with a transparent conducting oxide (TCO), which allows light to enter into the cell. Attached to the surface of the oxide there is a monolayer of dye molecules, which are responsible for harvesting the light. The sensitized film is surrounded by an electrolyte solution of high ionic strength, usually composed of an organic solvent containing a redox pair. Figure 2.7 depicts the components of DSSC.

The most successful combination of materials is still the one reported in the pioneering work by the Grätzel group [8], which opened the research field of dye-sensitized solar cells. In this configuration the main components are a layer of nanoparticles sensitized by a ruthenium complex dye with I^-/I_3^- redox couple in an organic solvent, which acts as the redox mediator. Grätzel and O'Regan found a successful combination of a nanostructured semiconductor electrode with an efficient and stable dye.

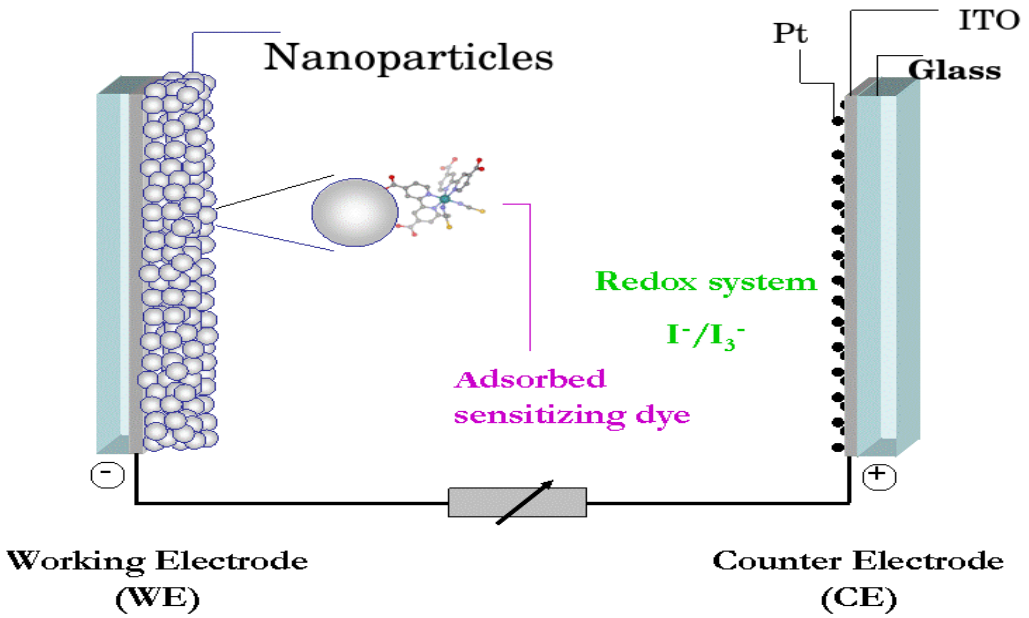

Figure 2.1: Schematic of DSSC.

The key factor of that combination, already pointed out for mesoporous semiconductor electrodes in 1976, was the surface area. In a mesoporous film, the incoming photons can be captured efficiently although the surface is covered only by a monolayer of dye. The reason is that a mesoporous structure can have a surface area available for dye adsorption more than a thousand times larger than a flat electrode of the same geometric area [9].

2.1 Working principles of DSSCs

Dye-sensitized solar cells are photoelectrochemical devices where several electron transfer processes run in parallel and in competition. In a dye sensitized solar cell optical absorption and charge generation are separate functions. The role of dye molecules is the same as that of chlorophyll in leaves, they must absorb the incident sunlight and induce an electron transfer reaction. A scheme of the basic working principles of DSSC is given in Figure 2.2.

Upon illumination the incident light is absorbed by the dye which is excited (1). From the excited state an electron can be injected into the conduction band (CB) of the semiconductor leaving the dye in its oxidized state (2). The extracted charge performs electrical work

in the external circuit (3), before it reaches the counter electrode. The oxidized species in the electrolyte are regenerated at the counter electrode (4) and the circuit is closed by the reduction (regeneration) of the dye by electron transfer from the electrolyte (5).

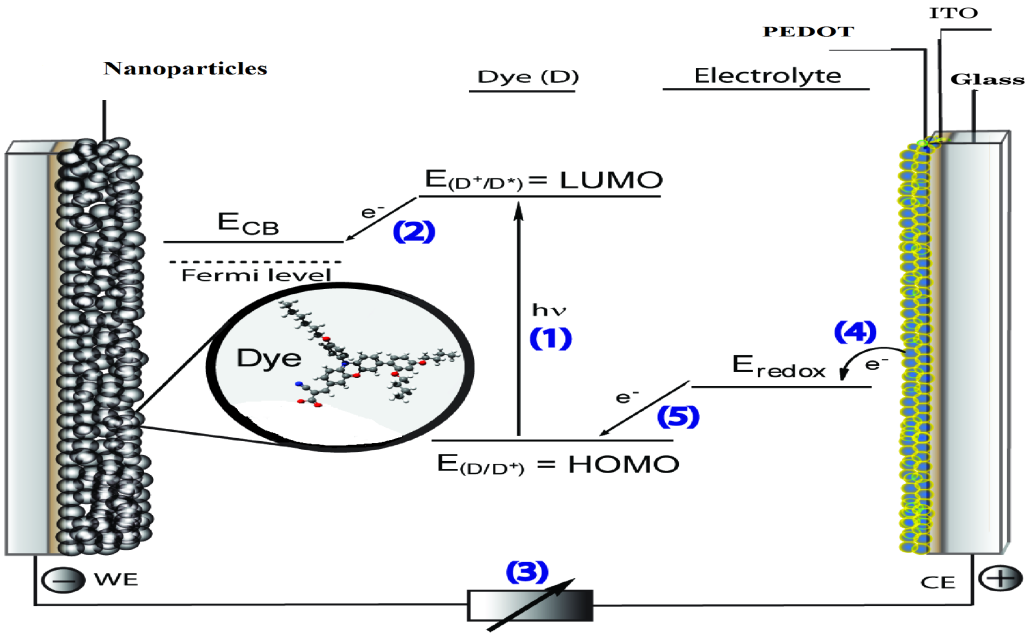

Figure 2.2: Overview of the working principle of DSSCs.

The regeneration of the sensitizer by iodide intercepts the recapture of the conduction band electron by the oxidized dye. The iodide is regenerated in turn by the reduction of triiodide at the counter electrode, the circuit being completed *via* electron migration through the external load. The theoretical maximum voltage that such a device could deliver corresponds to the difference between the redox (Nernst) potential of the mediator and the quasi-Fermi level of the electron in the semiconductor.

Two important processes involving in the dye are electron transfer from the excited dye into the conduction band of the nanoparticle referred to as the electron injection and reduction of the oxidized dye by the redox mediator, which is called dye regeneration, see Figure (2.2). For efficient electron injection the excited state of the dye, $E_{(D^+/D*)}$, needs to be at more negative potentials compared to the accepting conduction band edge, E_{CB}, of the semiconductor. For efficient dye regeneration the redox potential of the redox mediator, E_{Redox}, needs to be at less positive potentials than the redox potential of the dye ground state, $E_{(D/D^*)}$.

For an electron transfer reaction to be viable over other competing reactions it must be favored both by appropriate energetics and kinetics. After successful electron injection the dye is oxidized and can be reduced either by electrons of nanoparticle or by the redox donor in the electrolyte. The time for dye regeneration should be shorter than the time to recombine to the oxidized dye. After electrons are injected into the semiconductor nanopartilce, the electrons should preferentially be transported to the back-contact, where they can be extracted to perform electrical work. During the transport through the porous semiconductor network the electrons can recombine to either the oxidized dye or to triiodide.

2.2 Materials of dye-sensitized photoelectrochemical cell

The components of the dye-sensitized solar cells have changed relatively little since its inventing. The development has concentrated on the one hand to the tuning of the properties of the original components, such as the morphology and surface properties of the semiconducting electrode and the chemical composition of the electrolyte. On the other hand new alternative materials and methods such as solid electrolytes and plastic substrates have been explored.

2.2.1 ZnO semiconductor

The semiconductor oxide is the physical support of the sensitizer molecules and the electron conductor in a dye-sensitized solar cell. As mentioned before, the mesoporous structure of the films is crucial for a high dye loading in the semiconductor. The wide bandgap semiconductor titanium dioxide has been by far the most widely used DSSC photoelectrode material. Titanium dioxide is a very versatile, non-toxic, cheap, and chemically stable material and its suitability for dye-sensitized solar cells has been extensively proved [1]. Many other wide bandgap oxide semiconductors have been also explored as potential electron conductors in DSSCs. However, up to now, no other semiconductor material has reached efficiencies comparable to titanium dioxide. Nevertheless, some semiconductors

present special characteristics that make them very attractive candidates as alternatives to titanium dioxide. These are oxide materials like SnO_2, In_2O_3, and ZnO that have been widely used as photoelectrodes for DSSCs. Among these materials ZnO is getting more attention because of the similar energy level position of the conduction band as for TiO_2 [10]. However, ZnO presents a much higher electron mobility than anatase TiO_2, which should favour electron conduction [11, 12].

Historically, ZnO was one of the first semiconductors used in dye-sensitized solar cells. The bandgap and conduction band edge of ZnO is similar to that of TiO_2 (anatase). ZnO has a higher electron mobility than TiO_2, which should favor electron transport. The use of ZnO in DSCs has increased dramatically in recent years. This can be mainly attributed to the relative ease of synthesizing highly crystalline ZnO (in the wurtzite structure) with different morphologies, such as nanoparticles, nanowires, nanorods, nanotubes, tetrapods, nanoflowers, nanosheets, and branched nanostructures.

Zinc oxide is a direct wide bandgap semiconductor with a large and diverse application potential. It crystallizes in wurtzite, zinc blende, and rocksalt structure. At ambient conditions, the thermodynamically stable phase is wurtzite hexagonal structure, where each anion is surrounded by four cations at the corners of a tetrahedron and *vice versa*. The relatively open structure of zinc oxide allows plenty of sites to accommodate intrinsic defects and extrinsic dopants [13]. ZnO with a wurtzite structure is naturally an n-type semiconductor. ZnO has a relatively poor chemical stability and it is nearly insoluble in water but soluble in acids or alkalies. It is considered as amphoteric oxide. Its reaction depends on the pH of the media.

In acidic solution: $ZnO + 2H^+ \rightarrow Zn^{2+} + H_2O$

In basic solution: $ZnO + H_2O + 2OH^- \rightarrow [Zn(OH)_4]^{2-}$

The best result for a ZnO DSSC upto now was achieved by Saito and Fujihara [14], who obtained a 6.58% of overall efficiency. This is about half of the maximum efficiency obtained for TiO_2 [15]. The mesoporous layer of ZnO is deposited on a transparent conducting oxide (TCO), on a glass or plastic substrate. TCO is an important material not just

for solar cells but also for various applications especially in the optoelectronic field, such as flat panel displays, LEDs, and waveguide devices. TCO is a wide bandgap n type semiconductor that consists of high concentration of free electrons. The most common ones are Indium doped tin oxide (ITO), fluorine doped tin oxide (FTO) and aluminium doped zinc oxide (AZO or Al:ZnO) due to the good electrical conductivity, high transparency and the low material costs. In case of ITO, when it is placed at temperature over 300^0C, its conductivity drops dramatically. This is due to the decrease in oxygen vacancies in high temperature, resulting in the decrease of electric carriers.

ZnO has a wide bandgap (3.2 eV), with limited photo-catalytic applications to shorter wavelengths (it demands UV light). But only about 4% of the solar spectrum falls in the UV region, so ZnO semiconductor performance under solar light must be improved. Using small bandgap semiconductors instead is not an alternative, because they are unstable [16]. In order to improve zinc oxide properties as semiconductor and photocatalyst under solar light; studies have been made to sensitize ZnO by adding another element. The sensitization of ZnO by natural dye is an alternative because it is safe, cheap, and ecofriendly with nature [17]. The dye has a small bandgap and absorbs light wavelengths in the visible region. This leads to electron-hole generation in the dye molecule, by exciting the electrons from dye HOMO to LUMO. Charge transfer from dye LUMO to ZnO conduction band occurs.

Synthesis of ZnO nanoparticles

Various types of ZnO synthesis techniques have been formulated over the years. ZnO nanostructures can be synthesized by several methods such as sputtering technique, vapour deposition, pulsed laser deposition (PLD), metal organic chemical vapour deposition (MOCVD), sol gel method vapour liquid-solid process, and anodization. Unfortunately, many of the stated techniques are problematic, needing high temperature for synthesis, and having long reaction time, utilize toxic components, and involve costly equipments. The sol-gel method is a simple, low-cost and most commonly used technique for the synthesis of ZnO nanostructures.

An alkaline solution is essential for the formation of ZnO nanostructures because normally divalent metal ions do not hydrolyze in acidic environments [18, 19]. The commonly used alkali compounds are KOH and NaOH. Generally speaking, the solubility of ZnO in an alkali solution increases with the alkali concentration and temperature. Supersaturation allows a growth zone to be attained [19]. KOH is thought to be preferable to NaOH, because K^+ has a larger ionic radius and thus a lower probability of incorporation into the ZnO lattice [20]. Furthermore, it has been suggested that Na^+ is attracted by the OH^- around the nanocrystal and forms a virtual capping layer, thus, inhibiting the nanocrystal growth [21].

The main reactions involved in the growth are given in Equations 2.1 to 2.5 [19]. For the Equation (2.2), the product is not necessarily $Zn(OH)_4{}^{2-}$, but could also be $Zn(OH)^+$, $Zn(OH)_2$, or $Zn(OH)_3{}^-$, depending on the parameters, such as the concentration of Zn^{2+} and the pH value.

$$Zn^{2+} + 2OH^- \leftrightarrows Zn(OH)_2 \tag{2.1}$$

$$Zn(OH)_2 + 2OH^- \leftrightarrows [Zn(OH)_4]^{2-} \tag{2.2}$$

$$[Zn(OH)_4]^{2-} \leftrightarrows ZnO_2^{2-} + 2H_2O \tag{2.3}$$

$$ZnO_2^{2-} + H_2O \leftrightarrows ZnO + 2OH^- \tag{2.4}$$

$$ZnO + OH^- \leftrightarrows ZnOOH^- \tag{2.5}$$

At the very beginning of the growth process Zn^{2+} and OH^- ions coordinate with each other, and then they undergo dehydration by proton transfer, forming Zn^{2+} ... O^{2-} ... Zn^{2+} bonds, and leading to an agglomerate. These aggregates usually contain fewer than 50 ions, and the formation of O^{2-} ions implies dramatic changes within the aggregate. After the aggregates reach around 150 ions, wurtzite type (tetrahedral coordination) ZnO domains are then nucleated in the central region of the aggregates [22]. Aggregates of over 200 ions exhibit a nanometer sized core of the wurtzite structured ZnO which grows

as a result of further association and dehydration of Zn^{2+} and OH^- ions [23].

In Equations 2.1 to 2.5, the O^{2-} in ZnO comes from the base, not from the solvent H_2O. Therefore growth of ZnO does not necessarily require the solvent to be H_2O [22]. It could be organic solvents, such as methanol, ethanol, butanol etc. Under alkali conditions, the reactions could take place at room temperature by adjusting the ratio of Zn^{2+} and OH^-, giving rise to ZnO nanowires with diameter even below 10 nm. ZnO nanowires with various aspect ratios can be prepared by simply adjusting OH^- concentration and reaction time [24].

In this work, ZnO nanoparticles were synthesized by the hydrolysis of zinc salt according to the method developed by X.Y Shen et al [25] with little modification and along with heating at 120^0C. Zinc acetate and sodium hydroxide was used as raw materials, while polyethylene glycol employed as dispersant agent.

Size determination of ZnO nanoparticles

In the dilute concentration limit the particle size distribution and the total particle concentration can be found from the absorbance spectra. Pesika et al. [26] confirmed that the particle size distribution obtained from the absorbance spectra was in excellent agreement with the particle size distribution obtained from TEM images of the same zinc oxide particles. The particle size distribution can be determined from the UV-absorbance spectra because when the crystal size approaches the exciton diameter quantum confinement affects the electronic structure and widens the bandgap of the particles. The bandgap widening is related to the particle diameter; the smaller the particles the larger the widening. In an ensemble of nanoparticles with diameters in the quantum confinement regime, each particle size starts absorbing radiation at different wavelengths.

The largest particles will start absorbing at the longest wavelengths and as the wavelength decreases the smaller particles will start to absorb until all the particles are absorbing at the peak of the absorbance spectra [26]. The variation in the wavelength at which the particles in the ensemble start to absorb broadens as well as blue-shifts the absorbance

spectra as compared to the bulk crystal absorbance spectra. This change in the shape of the absorbance spectra is used to find the particle size distribution.

The effective mass model for spherical particles, derived by Brus [27, 28], quantifies the bandgap widening and relates the bandgap energy, E^{nano}, of a particle to its radius R, by Equation 2.6. According to the effective mass approximation model the bandgap of semiconductor nanoparticles (which is considered as a sphere with radius R) is given by bandgap of spherical particles. The average particle size in suspension can be obtained from the absorption maxima and the corresponding wavelength in which, maximum absorption occurs, because it is possible to determine $E_g{}^{nano}$ from the wavelength. Using the effective mass model where the bandgap (eV) can be approximated by

$$E_g^{nano}(R) = E_g^{bulk} + \frac{h^2}{8m_0R^2}(\frac{1}{m_e^*} + \frac{1}{m_h^*}) - \frac{1.8e^2}{\varepsilon_0\varepsilon_r R} \tag{2.6}$$

Where E_g^{bulk} is the bulkband gap value, h is plank's constant, m_o the electron mass, while m_e and m_h are the electron and hole relative effective mass, respectively, e the electron charge, ε_0 the permittivity of vacuum and ε_r the relative dielectric constant of the semiconductor. On the basis of Equation 2.6 the bandgap shift with respect to the bulk value is given by:

$$\Delta E_g = \frac{h^2}{8m_0R^2}(\frac{1}{m_e^*} + \frac{1}{m_h^*}) - \frac{1.8e^2}{\varepsilon_0\varepsilon_r R} \tag{2.7}$$

The first term in Equation 2.7 referred to as the quantum localization term (i.e. the kinetic energy term), which shifts the E_g(R) to higher energies proportionally to R^{-2}. The second term in Equation 2.7 arises due to the screened coulomb interaction between the electron and hole, it shifts the E_g(R) to lower energy as R^{-1} [27]. From Equation 2.7 we can calculate the average radius of nanoparticle (R)

$$R = \frac{-(\frac{1.8e^2}{\varepsilon_0\varepsilon_r}) + \sqrt{(\frac{1.8e^2}{\varepsilon_0\varepsilon_r})^2 + (E_g^{nano} - E_g^{bulk})\frac{h^2}{2m_o}(\frac{1}{m_e^*} + \frac{1}{m_h^*})}}{2(E_g^{nano} - E_g^{bulk})} \tag{2.8}$$

2.2.2 Sensitizers

The semiconductor oxides used in DSSCs are wide bandgap materials, which do not absorb in the visible region. The function of harnessing the solar light is carried out by the sensitizer molecules attached to their surface. The absorption spectrum of the optimum dye for DSSCs should cover the whole visible region and even part of the near infrared. In addition, the dye must have suitable anchoring groups, which firmly attach the molecule to the semiconductor oxide.

The classic sensitizer dye employed in DSSCs is a ruthenium dye, which is usually referred to as N3, or in its partially deprotonated form (a di-tetrabutylammonium salt) as N719 [29]. Figure 2.3 shows the chemical structure of this dye. The incorporation of carboxylate groups allows ligation to the film surface *via* the formation of bidendate and ester linkages, whilst the (NCS) groups enhance the absorption of visible light. Adsorption of the dye to the mesoporous film is achieved by simple immersion of the nanocrystalline film in a solution of dye, which results in the conformal adsorption of a dye monolayer to the film surface.

The monolayer of the sensitizer is adsorbed to the surface of the semiconductor by chemical bonding. The function of the sensitizers is to absorb the incident light, inject the excited electron into the semiconductor, and become regenerated by the redox couple in the electrolyte. Numerous metal complexes and organic dyes have been synthesized and utilized as sensitizers. By far, the highest efficiency of DSSCs sensitized by Ru-containing compounds absorbed on nanocrystalline TiO_2 reached 11% [30].

Even if such DSSCs have provided a relatively high efficiency, there are several disadvantages of using noble metals in them, noble metals are considered as resources that are limited in amount, hence results in costly production, and they are not environmentally friendly. On the other hand, organic dyes are not only cheaper but have also been reported to reach a power conversion efficiency as high as 9.8% [31].

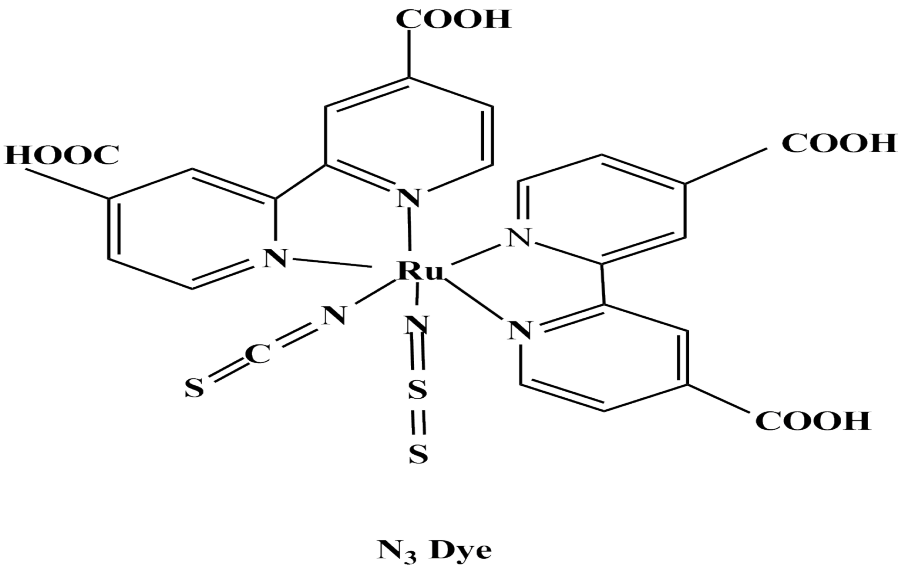

Figure 2.3: Chemical structure of the N_3 ruthenium complex.

In nature, fruit, vegetable, leaves, flowers, and algae contain several dyes which can be easily extracted and employed in dye sensitized solar cells. The use of natural pigments as sensitizing dye for the conversion of solar energy in electricity is interesting because, on one hand it enhances the economical aspect and, on the other, it has significant benefits from the environmental point of view. Natural pigments extracted from fruits and vegetables, such as chlorophyll, anthocyanins, and Betalains have been extensively investigated as sensitizers for DSSCs [32].

Chlorophyll derivatives

Chlorophyll is the major light-absorbing pigment in green plants. It is located within the membrane of the chloroplasts, which are small, green organelles which initiates photosynthesis by absorbing energy from sunlight and transferring this energy to other molecules. Chlorophyll has magnesium as its central metal ion, and the large organic molecule to which it bonds is known as a porphyrin. The porphyrin contains four nitrogen atoms bonded to the magnesium ion in a square planar arrangement (see Figure 2.4).

Chlorophyll occurs in a variety of forms but plants contain chlorophyll a and b. These two types of chlorophyll differ only slightly, in the composition of a side chain (in a it is CH_3, in b it is CHO). Both of these two chlorophylls are very effective photoreceptors

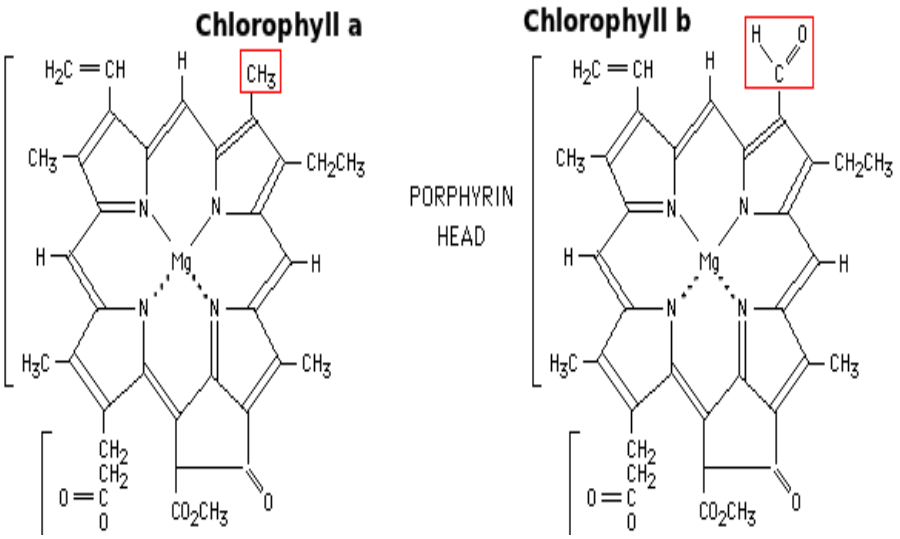

Figure 2.4: Structure of chlorophyll a and b.

because they contain a network of alternating single and double bonds, and the orbitals can delocalize stabilizing the structure. Such delocalized polyenes have very strong absorption bands in the visible regions of the spectrum, allowing the plant to absorb the energy from sunlight [32]. Chlorophyll absorbs light in the red (long wavelength) and the blue (short wavelength) regions of the visible light spectrum. Green light is not absorbed but reflected, making the plant appear green [29]. But even if chlorophyll absorb most of the blue and red light, the accessory pigments known as carotenoids can serve to enhance the absorption in the blue-green and yellow part of the spectrum.

In nature, carotenoids also act as energy transfer molecules for chlorophyll and prevent degradation of the molecules by quenching certain energy states, thus acting as photoprotectors [33]. Another interesting feature found in nature is the stacking of the thylakoid membranes (containing the chlorophyll) to enhance light absorption. Such stacking has similarities with the structure of the mesoporous network in a DSSC. These properties make photosynthetic pigments attractive to use as sensitizers in solar cells [34]. As mentioned before, these molecules become cation radicals and are susceptible to undesirable side reactions before being reduced by the electrolytic species [29].

Anthocyanin

Anthocyanins are one of the largest and most important group of water soluble pigment found in most species of plant kingdom. They are accumulated in cell vacuoles and are largely responsible for diverse pigmentation from orange to red, purple, and blue in flowers and fruits. Their color (red, purple or blue) changes with pH. They belong to a parent class of molecules called flavonoids [35]. Their functions in flowers, with bright red and purple colors, are adaptive for attracting pollinators.

In photosynthetic tissues (such as leaves and sometimes stems), anthocyanins have been shown to act as a sunscreen, protecting cells from high-light damage by absorbing blue-green and UV light, thereby protecting the tissues from photo-inhibition, or high-light stress [35]. Figure 2.5 shows some possible structures for different anthocyanins.

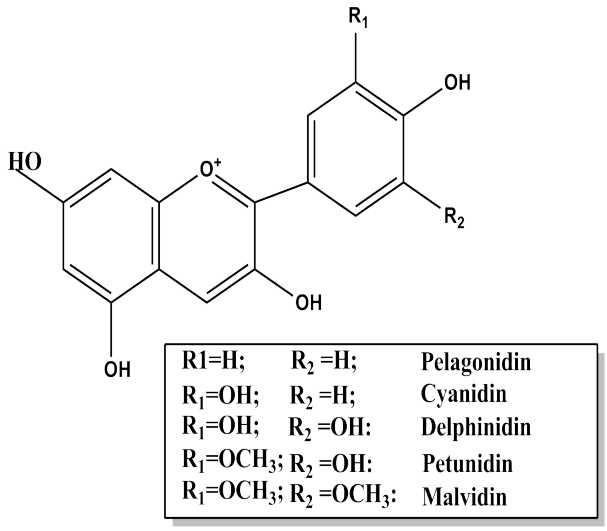

Figure 2.5: Basic chemical structures of most abundant anthocyanins.

Pigments of pelargonidin and cyanidin derivatives produce red and purple color, respectively, whereas those of delphinidin show purple or blue color [36]. The anthocyanidins are hydroxylated and methoxylated derivates of phenyl-2-benzopyrylium or flavylium salts, regarded as flavonoid compounds. Due to presence of eight conjugated double bonds carrying a positive charge, anthocyanins are intensely red or orange under acidic conditions (below pH 2), but in higher pH they are colorless and in alkaline conditions change their color into bluish. Intensity and type of the color of anthocyanins is affected

by the number of hydroxyl and methoxyl groups: if more hydroxyl groups, then the color goes toward a more bluish shade; if more methoxyl groups, then redness is increased [37].

Anthocyanin has small band gap (2.3 eV) and absorbs in the visible region. The absorption spectra depend on pH, at pH equal or below 2, anthocyanin solutions show characteristic maxima of absorption, one in the ultraviolet region (approximately 260 -280 nm) and two in the visible region (approximately 415 and 490 - 540 nm). The wavelengths of these absorbance peaks can differ slightly by a few nanometers among various anthocyanins, depending on structure of each anthocyanin. The maximum of absorption at 520 to 540 nm in the visible region is the most common wavelength used in the spectrophotometric measurement of total anthocyanins [38]. The solvent used for spectral determination affects slightly the position of the absorption bands, therefore it must be taken into consideration when comparing available data.

Anthocyanin pigment is a low cost dye, easily available, easy to extract and applicable without additional purifications. Moreover it has several carbonyls and hydroxyl groups that make it easy to anchor to the semiconductor surface [39]. All these reasons make anthocyanin vital alternative for synthetic dyes and most of other natural dyes.

Betalains

Betalain pigments represent an additional class of organic natural dyes of potential interest, they were extracted from beets and their name is even based on the word beet. These pigments are present in caryophyllale plants, have high molar extinction coefficients in the visible region and pH dependent redox properties. The pigments are present in the different parts of the plant including flowers petals, fruits, leaves, stems and roots.

The two main types of betalains that are present in plants are betcyanins and betaxantnines which absorbs light differently and gives a different spectrum of colour to the plants.Within these 2 categories, many subcategories are present. Betacyanins which are the reddish to violet betalain pigments, and betaxanthins which are the yellow to orange betalain pigments (see Figure 2.6) [40].

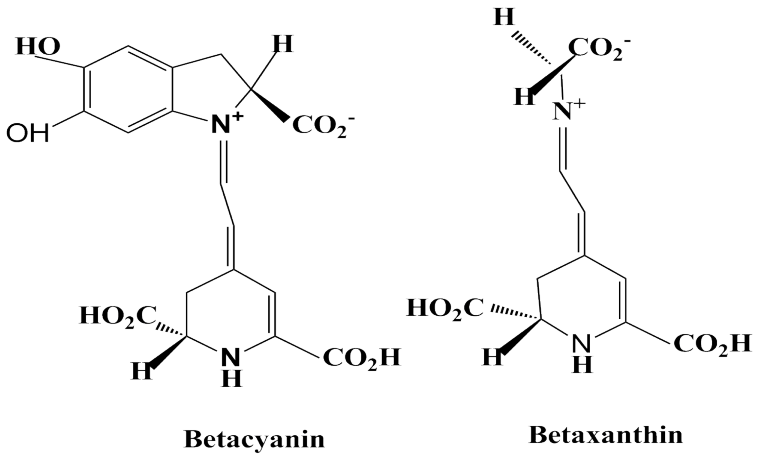

Figure 2.6: General structure of betalains: betcyanin and betaxanthin.

Generally pigments appear colorful because they selectively reflect and absorb certain wavelengths of visible light. White light is a roughly equal mixture of the entire spectrum of visible light with a wavelength in a range from about 380 or 400 nm to about 760 or 780 nm. When this light encounters a pigment, parts of the spectrum are absorbed by the chemical bonds of conjugated systems and other components of the pigment. Some other wavelengths or parts of the spectrum are reflected or scattered. Most pigments are charge-transfer complexes, like transition metal compounds, with broad absorption bands that subtract most of the colors of the incident white light.

When designing this natural dye for DSSC application, there are many important factors that need to be taken into consideration, some of them are :

- The dye should have a broad absorption spectrum, preferably all the way into the near-IR in order to harvest as many incident photons as possible.
- A high extinction coefficient will enable the use of thinner semiconductor films and still keep a high degree of absorbed photons.
- It must bind strongly to the semiconductor surface for long term stability.
- The energy levels should match the conduction band of the semiconductor and the redox potential of the electrolyte.
- Low toxicity and possibility to recycle.

- High photostability to sustain for many years of use.
- Achieve a long lifetime of the injected electrons by blocking the recombination pathways.

We have therefore use a procedure to extract the above pigments for the sensitizing ZnO nanocrystalline film. We use water and ethanol extracts of flowers of *Jacaranda mimosifolia, Bougainvillea spectabilis, Hibiscus sabdariffa*, leafs of *Amarathus iresine herbisiti*, roots of *Beta vulgaris* and fruits of *Carissa ovata* which contain pigments (anthocyanin, chlorophyll and betalians). The extraction methods will be described in the experimental part.

2.2.3 Electrolytes

The iodide/triiodide couple is by far the most popular redox mediator used in dye-sensitized solar cells (DSSCs). Record power conversion efficiencies of about 11% have been obtained using this redox couple [41]. The success of the iodide/triiodide couple in DSSCs can be attributed to its favorable kinetics. At the working electrode, iodide gives fast regeneration of the oxidized dye, typically on a microsecond time scale. On the other hand, recombination of the injected electrons in ZnO with the oxidized form of the redox couple (mainly present as triiodide) is very slow, typically on the millisecond time scale under operating conditions. Slow recombination kinetics are crucial for successful use of mesoporous electrodes in DSSCs. At the counter electrode, which is provided with a catalyst such as Pt nanoparticles, rapid electron-transfer kinetics are obtained with the I^-/I_3^- couple [42].

One of the major problem of liquid electrolyte is its low long-term stability, which is caused by organic solvent evaporation and leakage, high temperature instability, and difficulties in sealing. To overcome these problems, much effort has been made to replace liquid electrolytes with ionic liquids, solid or quasi-solid-state electrolytes including polymer gel electrolytes, p-type semiconductors, and organic conductive materials. The quasi-solid-state, or gel state, is a particular state of matter, neither liquid nor solid, or conversely

both liquid and solid.

Generally, a quasi-solid-state electrolyte is defined as a system which consists of a polymer network (polymer host) swollen with liquid electrolytes [43]. Owing to its unique hybrid network structure, quasi-solid-state electrolytes always possess, simultaneously, both the cohesive property of a solid and the diffusive transport property of a liquid. Namely, quasi-solid-state electrolytes show better long-term stability than liquid electrolytes do and have the merits of liquid electrolytes including high ionic conductivity and excellent interfacial contact property [44]. These unique characteristics of quasi-solid-state electrolytes have been actively developed as highly conductive electrolyte materials for DSSCs.

2.2.4 Counter electrode

Among the components of DSSCs, the function of counter electrode is to transfer electron from the external circuit back to the redox electrolyte and catalyzing the reduction of the triiodide ion (I_3^-) [45]. Platinum-coated transparent conductive oxide electrode is used as a counter electrode due to its excellent electrocatalytic activity for the I^-/I_3^- redox couple. However, platinum is a noble metal and relatively expensive. Therefore, the cost of the platinum counter electrode represents more than 40% of the whole DSSC cell cost regardless of its preparation method. Furthermore, the slow dissolution of platinum counter electrode in the corrosive I^-/I_3^- redox electrolyte deteriorates the long term stabilities of DSSCs [46].

Poly(3,4-ethylenedioxythiophene) has been widely investigated as an electronically conducting polymer. It can be easily electrodeposited onto a surface by the electro-oxidation of its monomer EDOT [47]. A Poly(3,4-ethylenedioxythiophene) (PEDOT) film in its oxidized form has been found to have high conductivity and stability at physiological pH [48]. When PEDOT was synthesized through electrochemical method, the electropolymerization conditions, such as the solvent, the electrode, supporting electrolyte, polymerization potential, and applied electropolymerization method, have important effects on

the properties of the PEDOT films. Recently, the PEDOT film always cooperated with other material as the counter electrode used in DSSCs, such as graphene-PEDOT-PSS [49]. In this work PEDOT coated ITO electrode was used as a counter electrode in which the PEDOT film can be an efficient mediator and enhance the efficiency of DSSC.

2.3 Performance parameter of dye-sensitized solar cells

The relevant techniques used for solar cell characterization are described in the next section. Techniques used to characterize the complete photoelectrochemical solar cell device are very important since the properties of all components are dependent on the complex interplay arising in a complete device. The techniques used provide appropriate illumination intensities close to real operation conditions of a solar cell.

2.3.1 Standard solar spectrum and solar irradiation

The power density at the surface of the Sun is 62 MWm^{-2} and it is reduced to 1353 Wm^{-2} at the point just above the Earths atmosphere [50]. Before reaching the ground, the radiation passes through the atmosphere, which modifies the solar spectrum, both intensity and energetic distribution. The irradiation that finally reaches the ground will depend on the length of the path the radiation must pass. This optical path is defined as Air Mass (AM), which takes into account the attenuation radiation suffers due to atmospheric absorption and depends on the position of the Sun. The Air Mass is defined as

AM=$\frac{1}{\cos(\theta)}$, where θ is the angle of elevation of the Sun (Figure 2.7). When the Sun is directly overhead the Air Mass is 1 (AM 1) and the irradiance reaching the Earth's surface is maximum.This atmosphere thickness should attenuate the solar spectrum to a mean irradiance of around 900 Wm^{-2} [50]. However, for convenience the standard spectrum is normalized so that the integrated irradiance of this spectrum per unit area and unit time is 1000 Wm^{-2} (known as 1 sun illumination). This light intensity is used for standard testing conditions. The "G" in AM 1.5 G stands for global, as it can be differentiated between direct radiation and global radiation, which takes into account also the diffuse

light than flat surfaces.

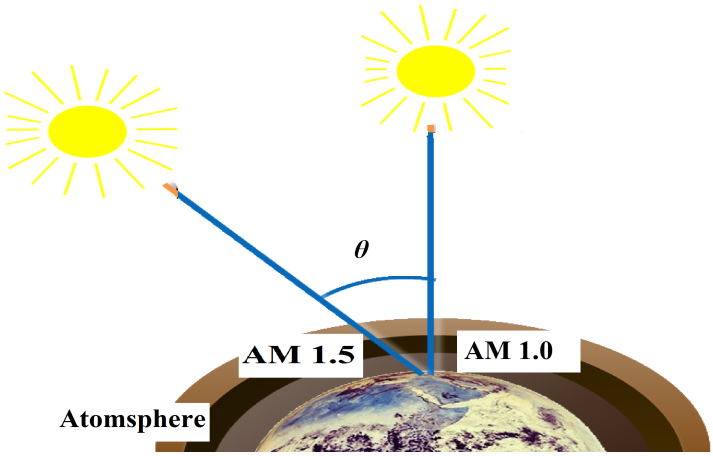

Figure 2.7: Schematic of AM 1.5, AM 1.0, and angle of elevation of the Sun.

2.3.2 Current-voltage characteristics

The solar cell efficiency is determined by its current-voltage (J-V) characteristics under standard illumination conditions. A standard solar spectrum of air mass 1.5 (AM 1.5) with an intensity of 1000 W/m^2 is used for characterization.

The V_{oc} is the difference in potential between the two terminals in the cell under light illumination when the circuit is open. It is dependent on both the Fermi level of the semiconductor and the level of dark current. The theoretical maximum of the cell is determined by the difference between the Fermi level of the semiconductor and the redox potential of the electrolyte. It is measured when the current through the cell is equal to zero (open circuit). Figure 2.8 shows an illustration of current-voltage characteristics of a cell under illumination. J_{sc} is the photocurrent per unit area (mA/cm^2). It is dependent on several factors such as the light intensity, light absorption, injection efficiency, and regeneration of the oxidized dye. It is strongly related to the incident photon to current conversion (IPCE) and theoretical values on the J_{sc} can be calculated from the IPCE spectrum. The maximum power generated is, when the product of the current and voltage is maximum, since the electrical power is given by the product of current density (J) times voltage (V).

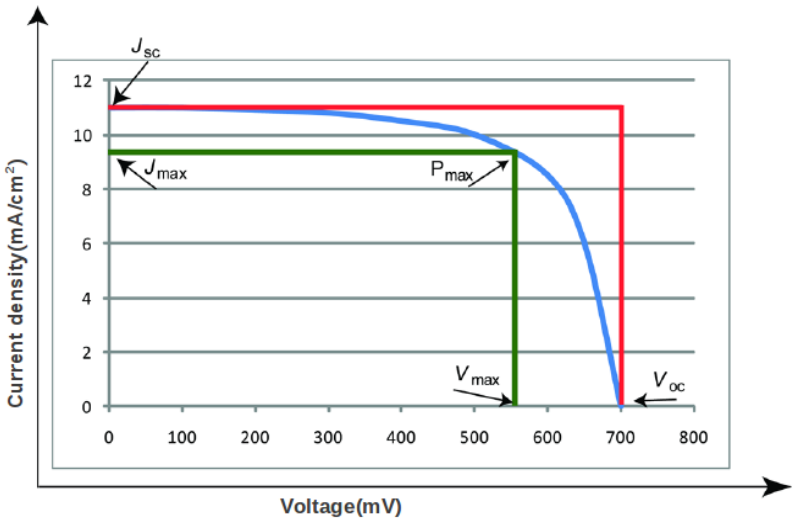

Figure 2.8: Current density *versus* Voltage characteristics of a DSSCs.

The degree of the squared shape of the J-V curve is given by the fill factor (FF), which measures the ideality of the device and is defined as the ratio of the maximum power output per unit area to the product of V_{oc} and J_{sc}.

$$FF = \frac{J_{(max.Power)}.V_{(max.Power)}}{J_{sc}.V_{oc}} \tag{2.9}$$

The solar to electric power conversion efficiency η is given by the ratio of the maximum extractable power to the incident solar power (P_{in}) given by Equation 2.11.

$$\eta = \frac{P_{max}}{P_{in}}, \eta = \frac{J_{max}.V_{max}}{P_{in}}, \eta = \frac{J_{sc}.V_{oc}.FF}{P_{in}} \tag{2.10}$$

Where P_{in} is the incident power, P_{out} is the output power, FF is the fill factor, η is the efficiency, J_{sc} is the short circuit current density, and V_{oc} is the short circuit voltage.

2.3.3 Incident photon to current efficiency (IPCE)

IPCE is one of the fundamental measurements of the performance of the solar. It is also known as the external quantum efficiency and describes how efficiently the light of a specific wavelength is converted to current that is (electrons out) / (photons in). The IPCE can be calculated according to equation [51].

$$IPCE(\%) = (\frac{1240.J_{sc}}{\lambda.P_{in}}).100 \tag{2.11}$$

J_{sc} is the short circuit current density, λ is the wavelength of the incident light and P_{in} is the intensity of the incident light. The factors determining the IPCE can be expressed as:

$$IPCE(\lambda) = \eta_{lh}(\lambda)\eta_{inj}(\lambda)\eta_{col}(\lambda) \tag{2.12}$$

where $\eta_{lh}(\lambda)$ is the light-harvesting efficiency of the sensitized oxide layer, $\eta_{inj}(\lambda)$ is the electron injection efficiency from the sensitizer into the oxide, and $\eta_{col}(\lambda)$ is the electron collection efficiency. The light harvesting efficiency of the sensitized films indicates how efficiently the adsorbed dye molecules harvest the incident light. The electron injection efficiency corresponds to the probability that a dye molecule in the excited electronic state injects an electron to the conduction band of the semiconductor. It thus determines how IPCE depends on charge separation at the dye/semiconductor interface. The charge separation depends, on the driving force for electron injection from the LUMO of the dye to the conduction band of the semiconductor oxide, but also, as recently reported [52], on the populations of the acceptor and donor levels in the injection process and the corresponding back process (electron dye-recombination).

The electron collection efficiency is an indication of the probability that a photogenerated electron reaches the collecting substrate contact before it is lost by recombination [51]. The collection efficiency thus depends on the average distance that electrons travel before recombination [53]. Figure 2.9 elaborate such parameters easily.

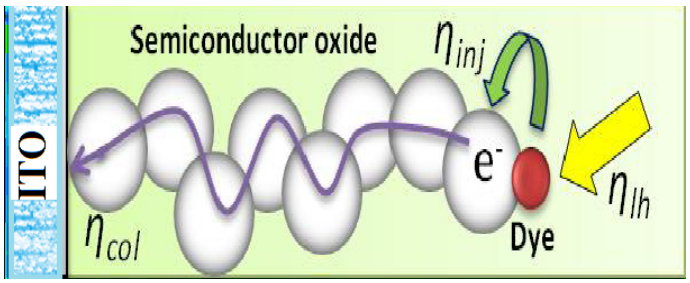

Figure 2.9: Scheme of the processes IPCE of DSSCs.

Chapter 3

Experimental

3.1 Synthesis of ZnO nanoparticles

Zinc acetate (B DH), sodium hydroxide pellets (Scharlau), and polyethylene glycol (Applied Science) were used as received. All the materials were first cleaned and rinse with distilled water and dried. All the chemicals were weighed with analytical balance and mixed in cleaned round bottom flask.

For the sol-gel method we used, 2.7 g of zinc acetate dehydrate and 0.5 g of polyethylene glycol (PEG) were taken and dissolved in in 250 ml of distilled water. 2 g of sodium hydroxide was dissolved in 500 ml of distilled water with vigorous stirring. The sodium hydroxide solution was added to the zinc acetate solution drop wise and the mixture was refluxed for 8 hrs at 120^0C using the setup shown in Figure 3.1.

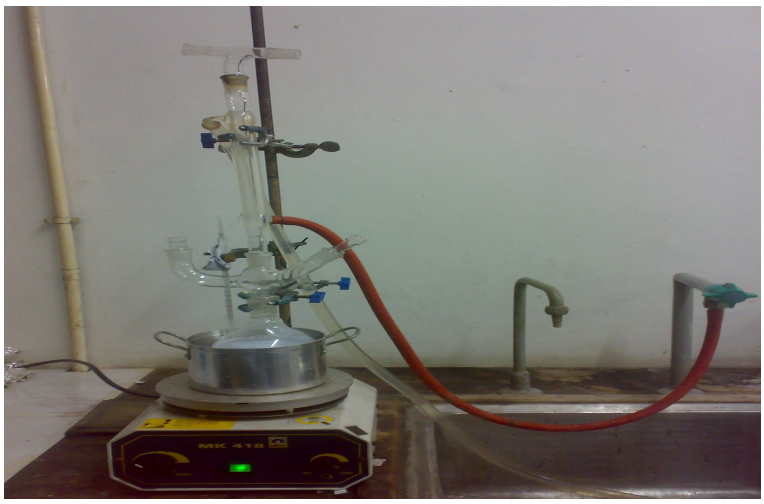

Figure 3.1: Experimental set-up for refluxing the solution.

The obtained ZnO solution was centrifuged to solid matter and solution. The solid matter was washed first by distilled water repeatedly, finally dried in Furnace to obtain ZnO. Diagrammatically the whole experiment can be summarized in Figure 3.2.

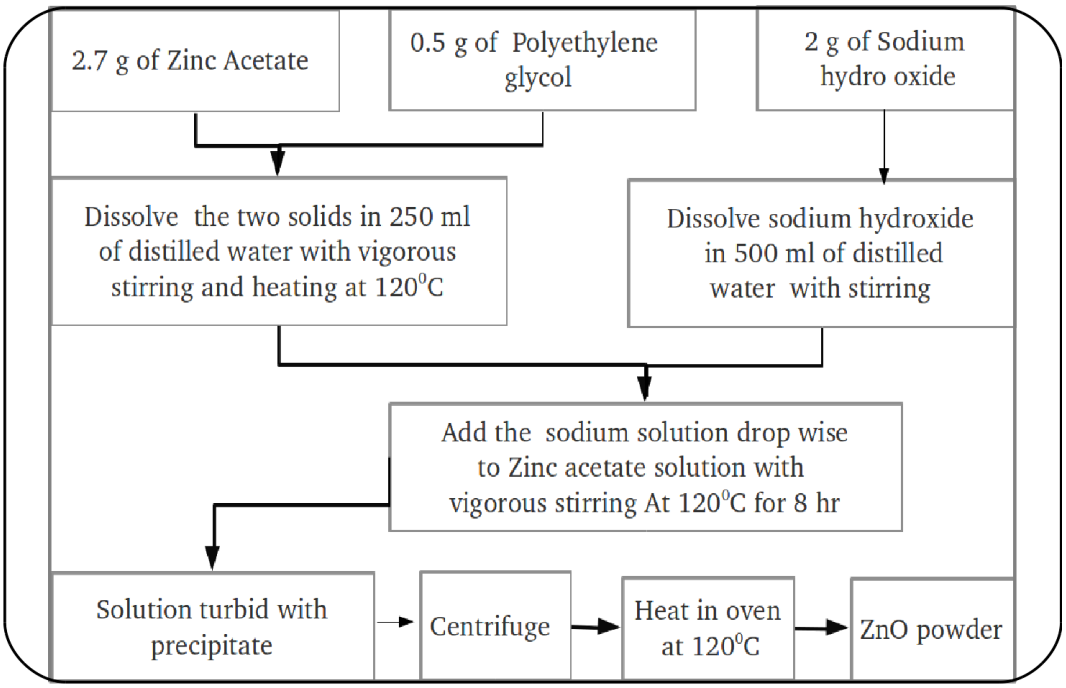

Figure 3.2: Steps of ZnO synthesis.

After preparing the coloidial nanopartciles optical absorption was done using Gensys-2 PC spectrometer to determine the size of colloidal nanoparticles. About 5 ml of the colloid were taken for measurement. Here for measurement the colloid nanopartciles were taken as soon as they reach the final temperature. We record the UV-visible absorption spectra between 275 and 500 nm. The solvent was used as a blank solution.

3.2 Natural dyes extraction

To select the dye that has good absorption in the visible region, fresh fruits, leaves, and flowers of plants including *Jacaranda mimosifolia, Beta vulgaris, Bouganvillea, Amarathus iresine herbisiti, Hibiscus sabdariffa, and Carissa ovata* collected. The collected plant was dried at room temperature in a shade to prevent pigment degradation (see Figure 3.3).

Figure 3.3: Fresh flowers and fruits under room temperature.

After drying for about 2 months the samples are completely dried in an oven at 70^0C to avoid some moisture from it. Then after, the samples were crushed with Micro Plant Grinding machine to produce the powder of the respective plant materials. The dye extraction from the powder was done as follows:

2 g of each powder sample was taken and soaked in 50 ml of ethanol for extracting using ethanol and in 50 ml water for extracting with water in separate bottle. The solution is stored at room temperature for about 6 hours to dissolve the powder completely. Then the solution were filtered with glass filter to separate the solid from the pure liquid. After filtration the the extracted pigment in different solvent are shown in Figure 3.4.

The pigment shown in Figure 3.4 are ready for soaking the electrode inside it, and also used for measuring the UV-vis absorption spectra. The absorption measurement was carried using the Gensys-2 PC spectrometer for each extract.

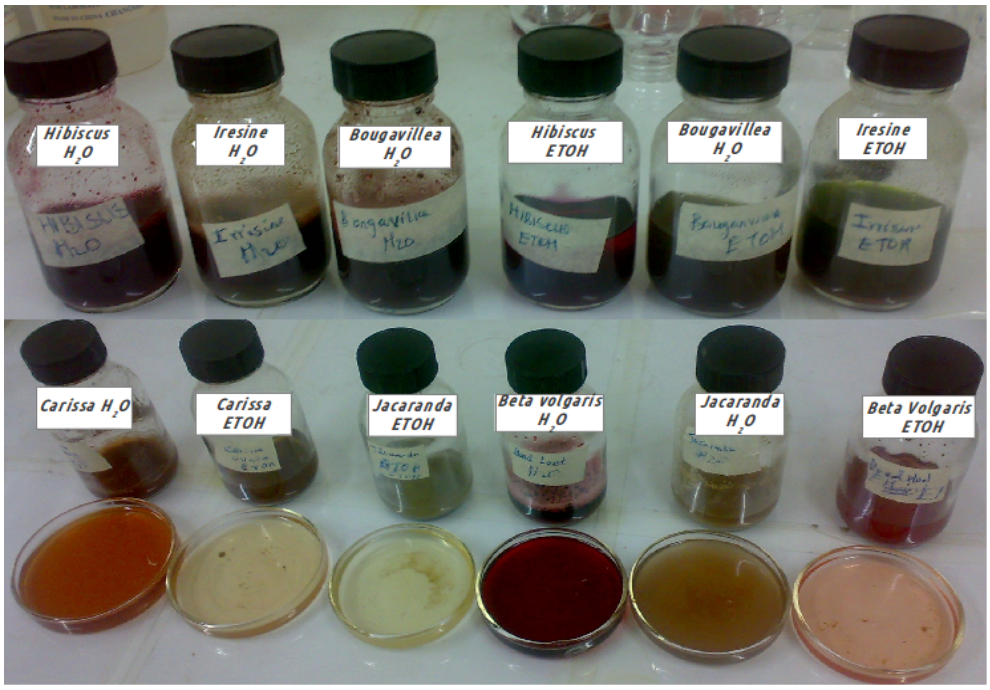

Figure 3.4: Samples of extracted pigment

3.3 Fabrication of dye-sensitized solar cells

The materials and the fabrication method employed for the fabrication of dye-sensitized Photoelectrochemical cells based on ZnO nanoparticles are described below.

3.3.1 Preparing the substrate for deposition

The substrate cleaning is believed to be a key process that influences the final performance of the devices. A significant effect on the photovoltage behavior can be observed experimentally depending on the extent of cleaning [54]. For this reason, TCO glass substrates have been thoroughly cleaned before film deposition. The glass cleaning protocol was, first cleaned with Acetone then with isopropanol finally with Ethanol. In all case the cleaning process was done in ultrasonic bath for about 20 minute in each solvent.

3.3.2 ZnO paste preparation

30 mg of polyethylene glycol (dispersing agent) and 10 ml of distilled water was mixed. 1.8 g of ZnO powder continuously grinded down by using procelain mortar to brake down

the aggregated particle. Then 2.5 ml of the PEG solution was slowly added to the powder and completely mixed with each other by using the mortar. Finally the paste was ready for deposition.

3.3.3 Deposition of ZnO films

The simplest and most widely used method for depositing ZnO paste on a substrate is the so-called doctor-blade method. The technique is also known as slot-coating in its mechanized version. It uses a hard squeegee, or doctorblade, to spread a portion of ZnO paste onto the glass (see Figure 3.5).

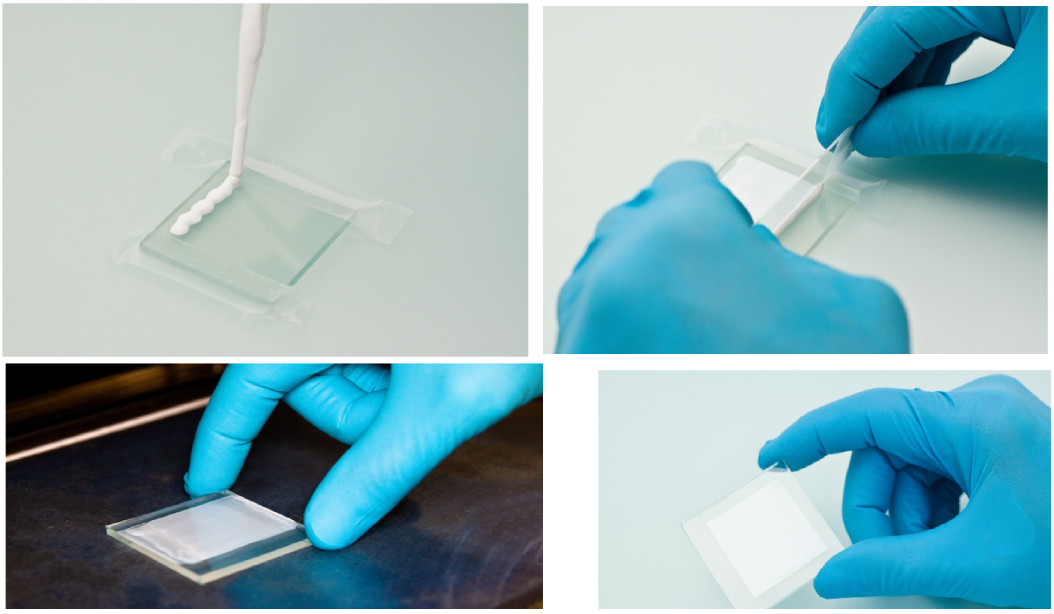

Figure 3.5: Deposition of ZnO oxide paste.

With the conductive side facing up, we apply four parallel strips of tape on the edges of the glass plate, covering about small portion of glass. After making the paste ready for deposition we apply the portion of paste near the top edge of the TCO glass between the two pieces of tape with the help of a glass rod, then, the paste spread across the plate with the support of the tape on all sides.

The preparation of electrode was completed by firing the deposited layer. The organic solvent burns away, leaving the ZnO nanoparticles sintered together. This process ensures electrical contact between particles and good adhesion to the TCO glass substrate. Sintering can occur in furnace at 400^0C.

3.3.4 Electrode sensitization

Natural dyes were used for electrode sensitization in the course of this thesis. Before immersion in the dye solution, films were warmed up to higher temperature (80^0C) to minimize the water vapour content inside the porous of the semiconductor electrode. The sensitization was always performed at room temperature. The best method of adsorbing a natural sensitizer to the oxide layer is by dipping the electrode in a solution of the dye already prepared. After sensitization, the films were rinsed in the same solvent (ethanol, water) as employed in the dye solution.

3.3.5 Prepartion of quasi-solid state electrolyte

The polymer gel electrolyte was prepared according to the method developed by L. Fan et al [55] as described below.

0.9 M of 1-ethylene-3-methyl immidazolium iodide (EMIM-I) was added into acetonitrile (Aldrich) under stirring to form a homogeneous liquid electrolyte. In order to obtain a better conductivity, 0.5 M of sodium iodide (BDH) was dissolved in the above homogeneous liquid electrolyte, and then 0.12M iodine and 35%(w/w) of PVP (Aldrich) were added. Then, the resulting mixture was heated at $70 - 80^0$C under vigorous stirring to dissolve the PVP polymer, followed by cooling down to room temperature to form a gel electrolyte.

3.3.6 Coating counter electrodes

A CHI630 Electrochemical Analyzer and a three-electrode electrochemical cell were used for polymerization of EDOT. The poly(3,4-ethylenedioxythiophene) (PEDOT) film for the counter electrode was formed by electrochemical polymerization of 3,4-ethylenedioxythiophene (EDOT) (Aldrich), in a three electrode one-compartment electrochemical cell. The electrochemical cell consisted of a pre cleaned ITO-coated glass working electrode, platinum foil counter electrode and quasi-Ag/AgCl reference electrode dipped in LiClO_4 (Aldrich) acetonitrile (sigma-Aldrich) solution.

The solution used for the polymerization contained 0.1 M EDOT and 0.1 M LiClO_4 in

acetonitrile (Sigma-Aldrich). The monomer was used as received. The polymerization was carried out potentiostatically at +1.8 V. At this potential, the electrode surface becomes covered with blue-doped PEDOT film. The film was then rinsed with acetonitrile and dried in air.

3.3.7 Assembly of DSSCs for characterization

Device assembly is the final step for characteristics measurement. Here the sensitized electrode was washed by the solvent of the dye then by ethanol and dried using hair dryer to dry the electrode, then the non covered part of the film by the paste was covered by a tape spacer in all side by leaving some place for electrical contact. By facing the active sides of the photoanode and the cathode, the two electrodes are pressed together after putting the quasi electrolyte on the photoanode. Then the devices are ready for characterization. The photoelectrochemical characterization was done by the experimental set-up depicted in Figure 3.6.

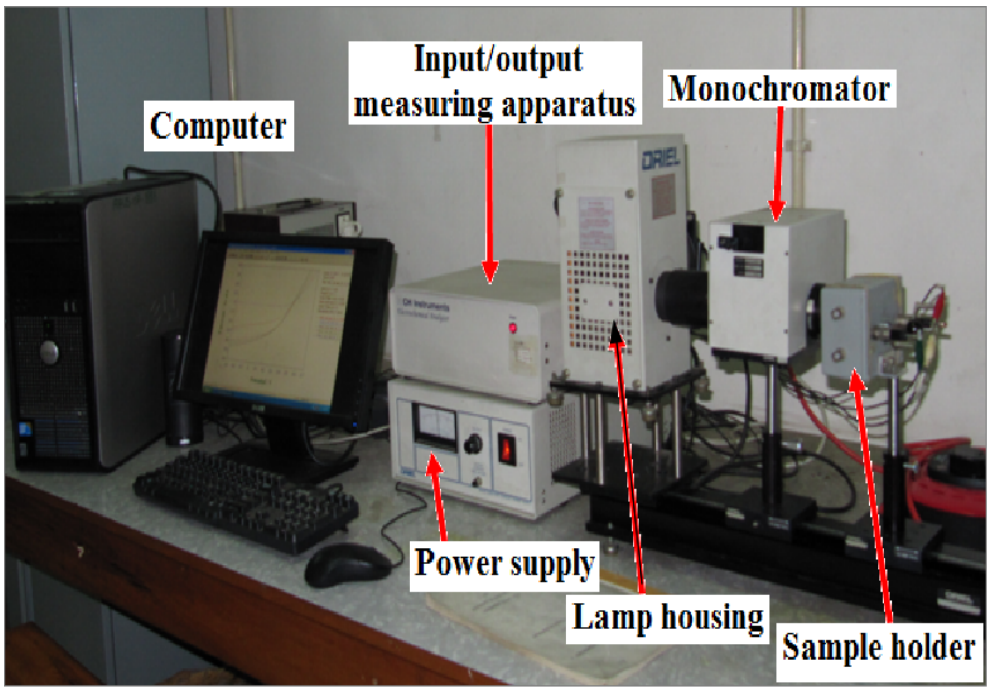

Figure 3.6: Experimental set-up for photoelectrochemical characterization.

Chapter 4

Results and discussion

4.1 ZnO nanoparticles size determination

Figure 4.1 is the plot of absorbance *versus* wavelength of the colloidal nanoparticles. From the absorption maxima the corresponding wavelength λ = 366 nm was obtained which is used for calculation of energy bandgap of nanoparticle.

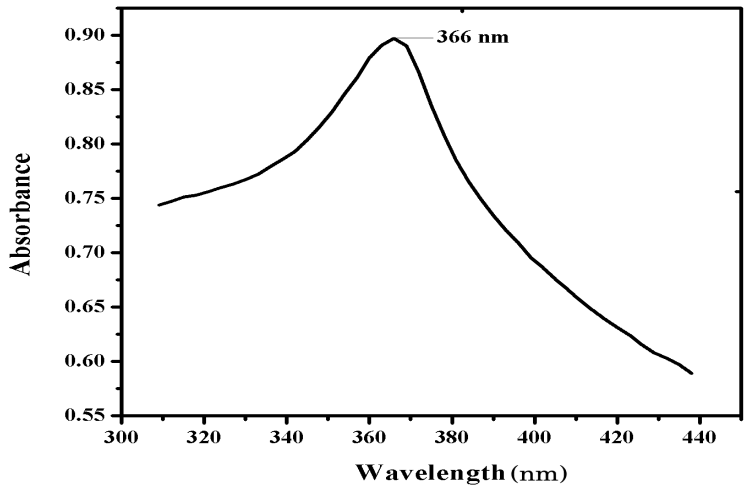

Figure 4.1: Plot of absorbance *versus* wavelength for colloidal ZnO nanoparticle.

Using this wavelength we can calculate the the energy bandgap of the nanoparticles E_g as:

$$E_g^{nano}(R) = E_g^{bulk} + \frac{h^2}{8m_0R^2}(\frac{1}{m_e^*} + \frac{1}{m_h^*}) - \frac{1.8e^2}{\varepsilon_0\varepsilon_r R} \tag{4.1}$$

Using the values $h = 6.626 \times 10^{-34} Js, E_g^{bulk} = 3.2eV, c = 2.998 \times 10^8 m/s, e = 1.602 \times 10^{-19} C, \epsilon_0 = 8.854 \times 10^{-12} \frac{C^2}{Nm^2}, m_0 = 9.110 \times 10^{-31} kg, \lambda_{max} = 366nm, \varepsilon_r =$

$8.66, m_e^* = 0.24, m_h^* = 0.59$ where m_0 is the rest mass of electron, m_e^* and m_h^* are the effective mass of electron and effective mass of hole, respectively [56]. So using the above given value we can calculate the radius of the nanoparticle as follows

$$R = \frac{-(\frac{1.8e^2}{\varepsilon_0 \varepsilon_r}) \pm \sqrt{(\frac{1.8e^2}{\varepsilon_0 \varepsilon_r})^2 + (E_g^{nano} - E_g^{bulk})\frac{h^2}{2m_o}(\frac{1}{m_e^*} + \frac{1}{m_h^*})}}{2(E_g^{nano} - E_g^{bulk})} \tag{4.2}$$

E_g^{nano}= 3.39 eV

Substituting all the given values in the above equation we have got the radius of the nanoparticle R=0.57 nm. Finally we would like to say that our nanoparticle prepared by the method which was mentioned in the experimental part has an approximate average particle size of 1.14 nm.

4.2 Optical absorption measurements

The absorption spectrum of the prepared dye, using the above method was measured by using the Genesys-2 PC spectrometer. Here first, some amount of the final dye solution was put in the quartz cuvett and the absorbance *versus* wavelength measurement was taken for each sample of ethanol and H_2O extract. And the graph of absorbance *versus* wavelength of each sample is shown in Figures 4.2 - 4.7.

Figure 4.2 shows the absorption spectra of *Bougainvillea spectabilis* extracted by water and ethanol. In water extract two peaks were found: the first one around 485 nm maximum absorbance which can be associated to the presence of indicaxanthin (which is a type of betaxanthin found in plant pigment), while the second one at 531 nm is attributable to the betanin pigment. Ethanol extract of *Bougainvillea spectabilis* shows an absorption peak at 664 nm which has also an absorption peak below 500 nm. From these peak it is clearly shown that ethanol extract contain both chlorophyll a and b which shows an absorption peak in between 400 - 500 nm and 600 - 700 nm [29].

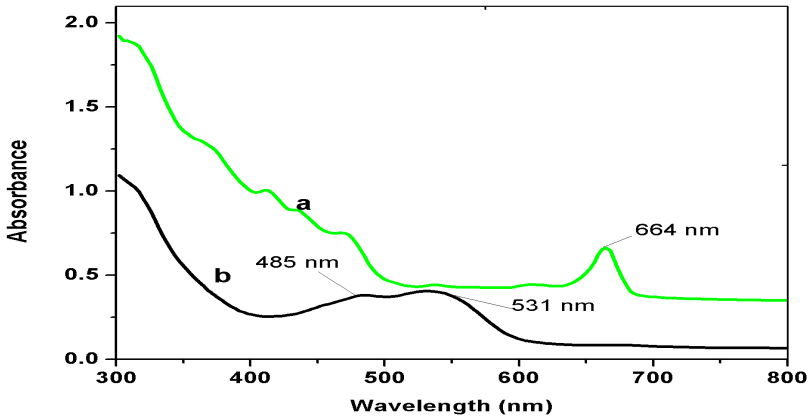

Figure 4.2: Absorption spectra of of *Bougainvillea spectabilis* extracted with a) ethanol b) H_2O.

The pigment extracted from *Carrissa Ovata* using water and ethanol shows an absorption peak at (553 nm, 664 nm), respectively (see Figure 4.3)

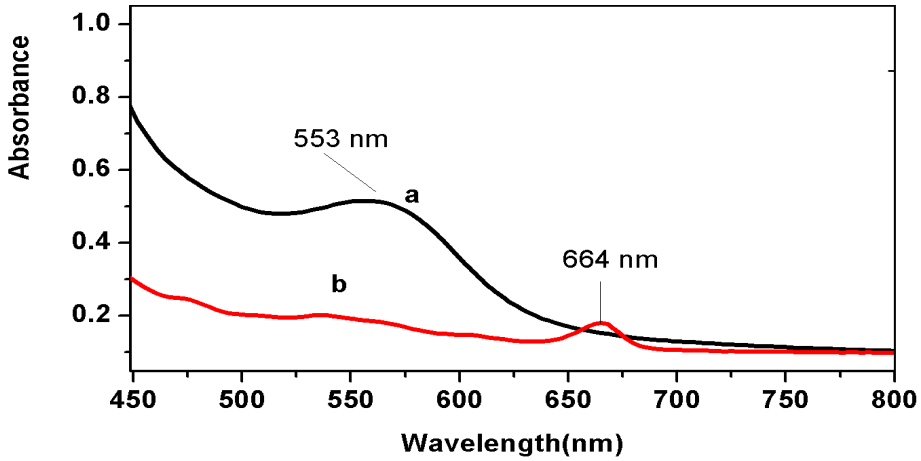

Figure 4.3: Absorption spectra of *Carissa Ovata* extracted with a) H_2O b) ethanol.

In ethanol extract of *carissa ovata* the extracted pigment was contain chlorophyll pigment which shows the characteristics absorption peak of chlorophyll. But the other spectra shows an absorption peak in the region of 520 - 550 nm which is the peak of anthocyanin containing dyes. This is because of the diverse pigmentation from orange to red, purple, and blue pigment which are found in anthocyanin containing pigment and shows an absorption in the visible region (approximately 490 - 550 nm) [36].

Ethanol and water extract of *Hibiscus sabdariffa* (Figure 4.4) shows absorption peaks at 549 nm and 519 nm respectively. The peaks are associated with presence of anthocyanin pigment. The difference in the absorption characteristics is due to the different type of anthocyanins and colors of the extracts.

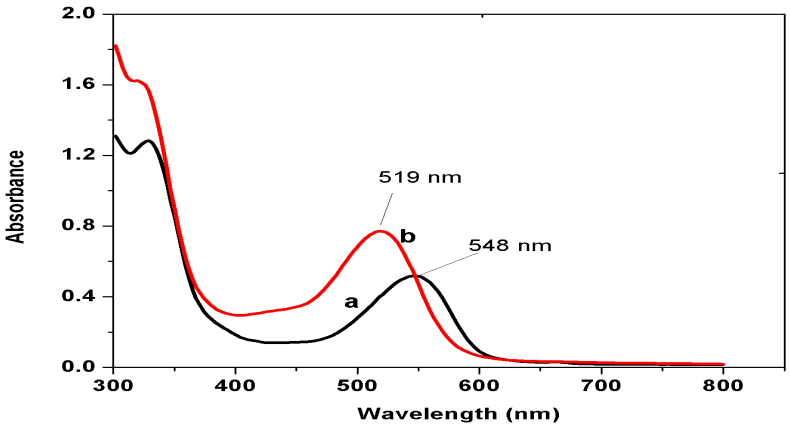

Figure 4.4: Absorption spectra of *Hibiscus sabdariffa* extracted with a) ethanol b) H_2O.

Beta vulgaris showed an intense absorption peaks in the region 400 - 600 nm . Here also both water and ethanol extract shows strong absorption peak of betalians, at 470 nm and 533 nm (Figure 4.5) due to the mixed contributions of the yellow-orange betaxanthins (480 nm) and of the red-purple betacyanines (540 nm) [40].

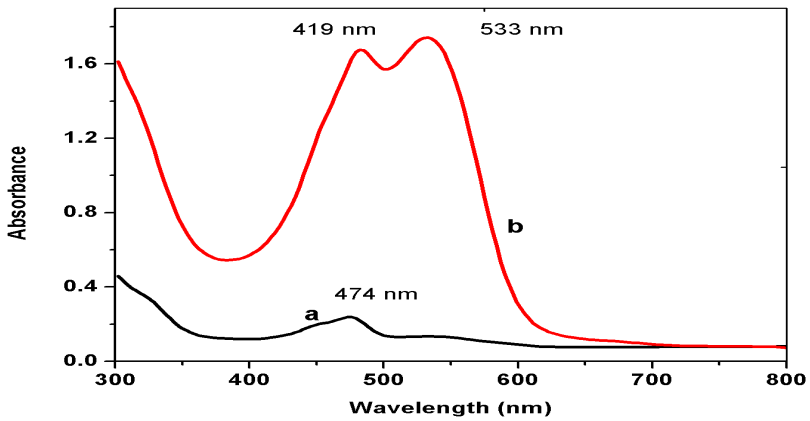

Figure 4.5: Absorption spectra of *Beta volgaris* extracted with a) ethanol b) H_2O.

In Ethanol extract of *Jacaranda mimosifolia* λ_{max} = 536 nm and water extract *Amarathus*

iresine herbisti λ_{max} = 532 nm, anthocyanin containing pigment were observed in the absorption spectra (see Figure 4.6 and 4.7). Ethanol extract of *Amarathus iresine herbisti* (λ_{max} = 433, 464, 664 nm) associated to the presence of chlorophyll which absorb most of the blue and red light.

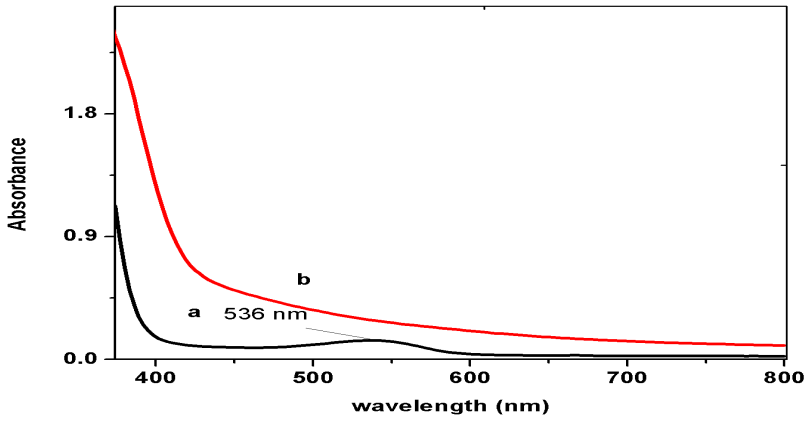

Figure 4.6: Absorption spectra of *Jacaranda mimosifolia* extracted with a) ethanol b) H_2O.

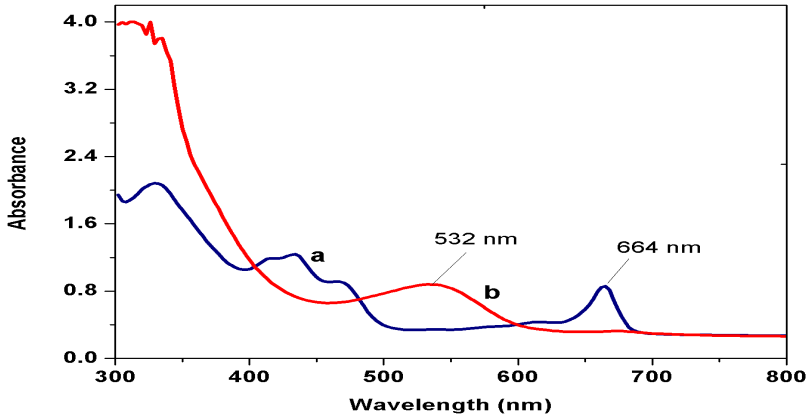

Figure 4.7: Absorption spectra of *Amarathus iresine herbisti* extracted with a) ethanol b) H_2O.

In Figure 4.6 water extract of *Jacaranda mimosifolia* doesn't show any absorption peak, this does not mean that there is no associated pigment. Instead it is because, the anthocyanin which can exist in two form, one in flavylium cation and the other quinonoidal

form, when the quinonoidal forms (Figure 4.8) are dominant the pigment did not show absorption maxima.

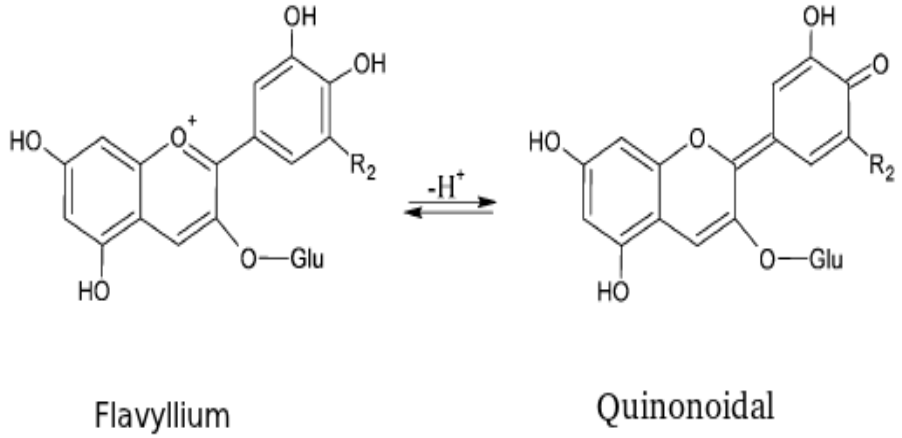

Figure 4.8: Equilibrium between flavyllium and quinonoidal

When this sample is acidified an absorption band which is a typical characteristics of anthocyanins starts to be observed due to the shift in equilibrium from quinonoidal to flavylium form. In this pigment, the aqueous environment, available in large quantity, add to the flavyllium form at pH values above 1.5 - 2.0, resulting in a loss of color owing to the formation of the colorless pigment through a slow acid-base equilibrium. This loss of color can be reversed by a simple re-acidification with complete recovery of the colored flavyllium cation. So that for the water extract of jacaranda the quinonoidal form of the anthocyanin is present in larger amount than the flavilum cation form.

Some of the wavelength of these absorbance peaks shows a red and blue shift by a few nanometers among various pigments, depending on structure of each and the solvent used for extraction of pigment. But in general the dye used in these studies are an effective photo-receptors because they contain networks of alternating single and double bond. When light is absorbed by the molecule of dye, the energy from the light excites an electron from its ground energy level to an excited energy level. Using suitable electron acceptor nearby, the excited electron can move from the initial molecule to the acceptor that is ZnO nanoparticles.

4.3 Current density *versus* voltage characteristics of ZnO based DSSCs

The J-V characteristic of all sensitizers were measured and plotted for analysis and comparison as shown below from Figure 4.9 - 4.14. In ethanol extract of *Beta vulgaris* Figure 4.9 the current density decreases as compared to the the water extract, but the reverse is true for the open circuit voltage. This is because of due to the low injection rate of electron into the semiconductor conduction band which decreases the short circuit current.

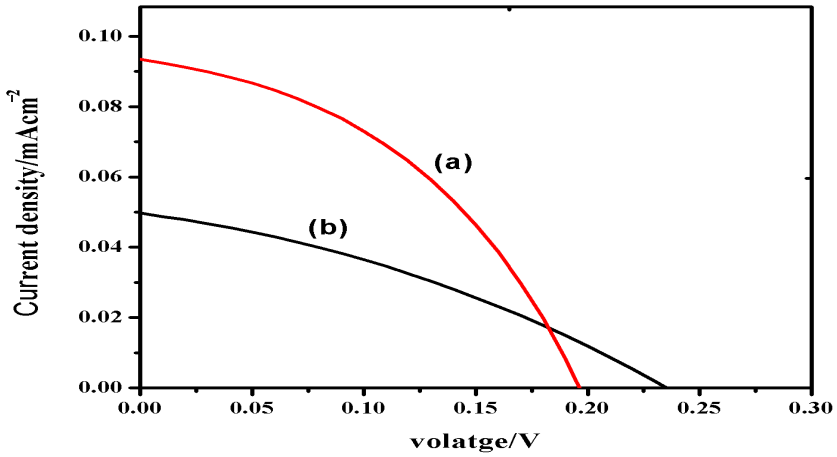

Figure 4.9: J-V of ZnO based DSSCs with *Beta vulgaris* sensitizers extracted by a) H_2O b) ethanol.

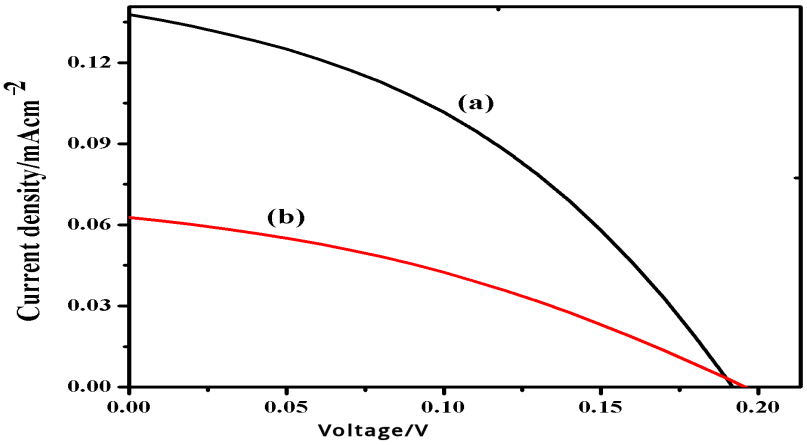

Figure 4.10: J-V of ZnO based DSSCs with *Hibiscus sabdariffa* sensitizers extracted by a) H_2O b) ethanol.

In Water extract of *Hibiscus sabdariffa* Figure 4.10 have showed better current than the corresponding ethanol extract with some increment in short circuit current density. In figure 4.13, Figure 4.14 for water and ethanol extract almost the they have the same short circuit voltage but the current density relatively higher for ethanol than the water extract which means that there is only a difference in electron injection efficiency.

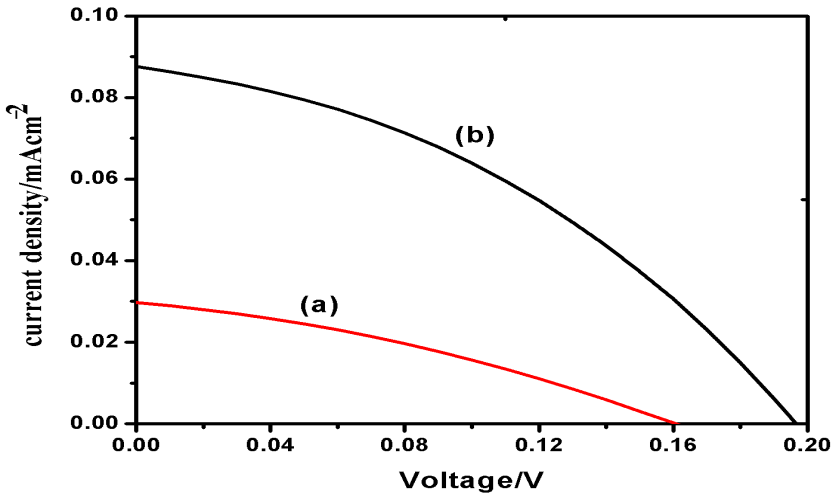

Figure 4.11: J-V of ZnO based DSSCs with *Bougainvillea* sensitizers extracted by a) H_2O b) ethanol.

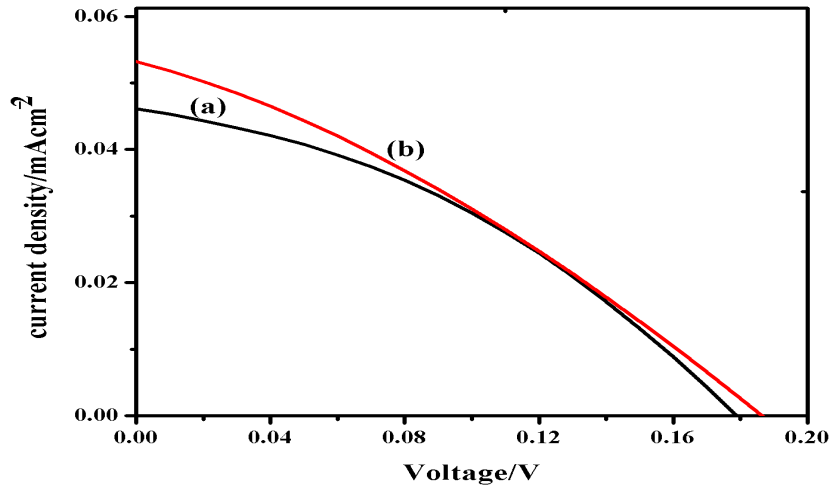

Figure 4.12: J-V of ZnO based DSSCs with *Carissa Ovata* sensitizers extracted by a) H_2O b) ethanol.

Most of the natural dye which have a good and a broader absorption in the visible spec-

trum is expected to shows a good rectification of the J-V curve that is responsible for good current density and power conversion efficiency. In these studies ethanol extract of *carissa ovata*, Figure 4.11, *Jacaranda mimosifolia* Figure 4.12, *bouganvilla spectabilis* Figure 4.13 and *Amarathus iresine herbisti* Figure 4.14, shows a better rectification which results relatively good photoelectrochemical performance for ethanol extract than the water extract.

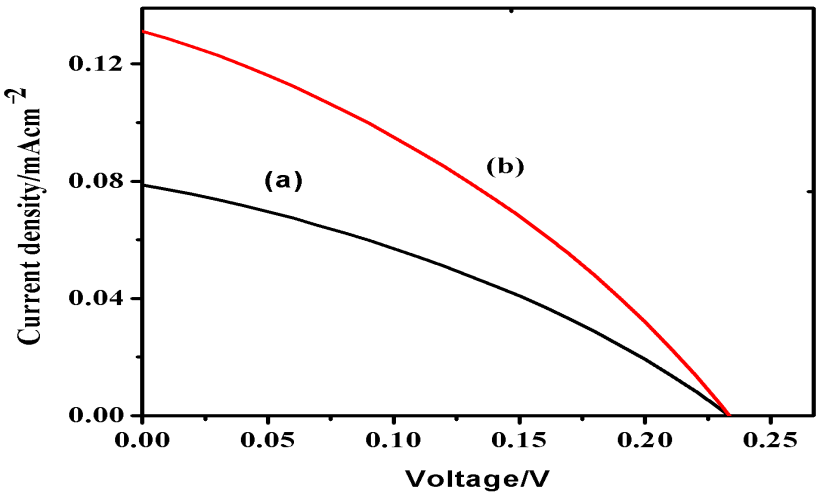

Figure 4.13: J-V of ZnO based DSSCs with *Amarathus Iresine* sensitizers extracted by a) H_2O b) ethanol.

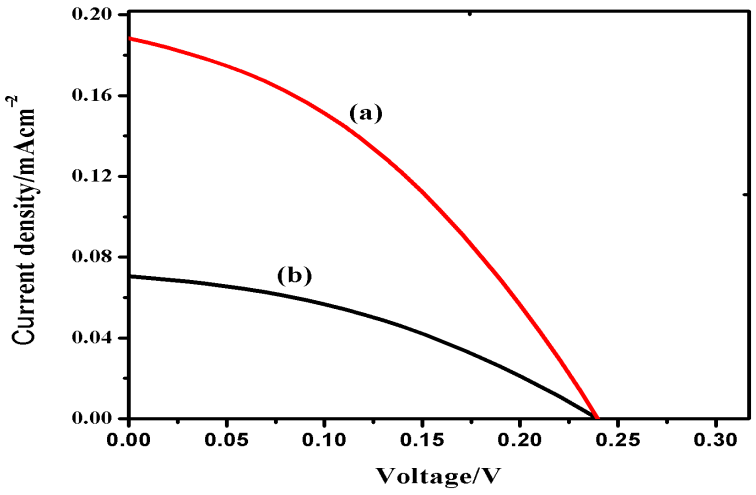

Figure 4.14: J-V of ZnO based DSSCs with *Jacaranda* sensitizers extracted by a) ethanol and b) H_2O

During the sensitization process (both ethanol and water extract of *Hibiscus sabdariffa* , *Bougainvillea spectabilis, carissa ovata*) we observed that, during socking the film starts to dissolve. This is because of protons derived from sensitizers make the dye solution relatively acidic which leads to the dissolution of the ZnO colloid [57]. The low local pH at the surface of ZnO during dye sensitization leads to the dissolution of Zn^{2+} ions from the ZnO surface (Figure 4.15(2)). These Zn^{2+} ions form complexes with the dye (Figure 4.15(2)), which accumulate in the pores of the semiconductor film. It is assumed that only dye molecules directly attached to the ZnO surface can inject efficiently electrons and contribute to the photocurrent [58]. Therefore, Zn^{2+}/dye complexes, in spite of absorbing light, do not inject electrons. So that the low current as well as low power conversion efficiency may arise arises due to this.

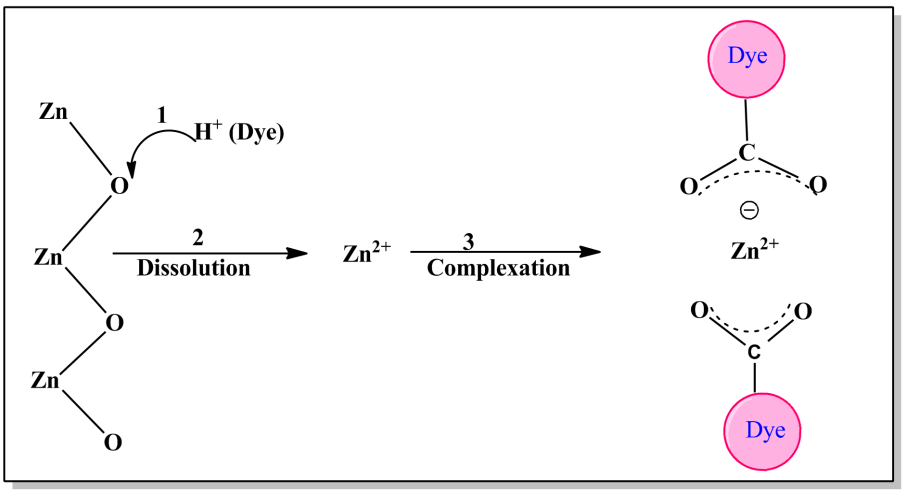

Figure 4.15: Zn^{2+}/dye complexes formation.

The instability of ZnO results from its surface properties in acidic dyes. In general, in a solution, the surface of the oxide is predominantly positively charged at a pH below the point of zero charge and negatively charged above this value, while the point of zero charge of metal oxides is defined as the pH at which the concentrations of protonated and deprotonated surface groups are equal. For example the ZnO sensitization process with Ru-complex dye, the (pH = 5) is much lower than the point of zero charge of ZnO (≈ 9). That means that the ZnO surface is positively charged. Thus, the protons adsorbed on the ZnO surface will dissolve the ZnO [59, 57].

Table 4.1 Summarized the performance of the DSSCs in terms of short-circuit photocurrent (J_{sc}), open-circuit voltage (V_{oc}), fill factor (FF), and energy conversion efficiency (η) compared to those of other extracts. The efficiency of cell sensitized by the *Amarathus iresine herbisti* extracted with ethanol was the best among the others. This is due to broader absorption range of the sensitizers, higher interaction between ZnO nano crystaline film and the pigment extracted from *Amarathus iresine herbisti* which leads to a better charge transfer. The current density and open circuit voltage it has higher value than the others which are 0.29 and 0.29 respectively. The fill factor also shows best value of 48.5% for ethanol extract of *Amarathus iresine herbisti*

Table 4.1: Photovoltaic performance of ZnO based DSSCs with different sensitizers

Sensitizers	Solvent	J_{sc} (mAcm^2)	V_{oc}	FF%	Efficiency
Carissa Ovata	Water	0.041	0.18	36.8	0.0027
	Ethanol	0.053	0.19	30.7	0.0031
Jacaranda mimosifolia	Water	0.038	0.16	33.0	0.0020
	Ethanol	0.071	0.24	37.4	0.0063
Beta vulgaris	Water	0.094	0.20	41.3	0.0077
	Ethanol	0.050	0.24	33.0	0.0039
Bougainvillea spectabilis	Water	0.030	0.17	31.5	0.0016
	Ethanol	0.088	0.20	37.4	0.0066
Hibiscus sabdariffa	Water	0.137	0.20	38.1	0.0104
	Ethanol	0.063	0.20	34.3	0.0043
Amarathus iresine	Water	0.079	0.24	32.6	0.0062
	Ethanol	0.290	0.29	48.5	0.0390

In literature it was reported that the extracting solvent has an effect on the efficiency of DSSCs [60]. The efficiency of the DSSCs was found to increase immensely when ethanol was used for extracting pigments [60]. In this study, similar finding was also obtained. This might be due to the fact that our extracted pigments are more soluble in ethanol and hence, the aggregation of dye molecules is less as expected. A good dispersion of dye molecules on the oxide surface could in fact improve the efficiency of the system.

4.4 IPCE characteristics of ZnO based DSSCs

Photoaction spectra (Figures 4.16 - Figure 4.20) provided further insights on the photoelectrochemical behavior of natural dyes. All the following figures shows the incident photon to current conversion efficiency (IPCE) spectra of ZnO electrodes sensitized with all of our extracted natural dyes as a function of wavelength. Some of the IPCE spectra of the organic dyes adsorbed on the ZnO electrodes are broader than the absorption curves of the dyes in solution.

Ethanol extract of *Bougainvillea spectabilis, Carissa ovata, Hibiscus sabdariffa, Jacaranda mimosifolia, Beta vulgaris* and *Amarathus iresine*, shows broad IPCE spectrum up to 610, 720, 430, 460, 550, 710 nm, respectively. And water extract of *Bougainvillea spectabilis, Carissa ovata, Hibiscus sabdariffa, Jacaranda mimosifolia, Bet vulgaris,* and *Amarathus iresine* from 300 up to 550, 730, 700, 460, 550, 650 nm, respectively, which showed some sensitization effect, but there spectrum is dominated by the spectrum of the ZnO nanoparticles. The IPCE of ZnO sensitized by *carisa ovata* and *Hibiscus sabdarifffa* shows a red shift on the absorption onset for water extract than ethanol extract.

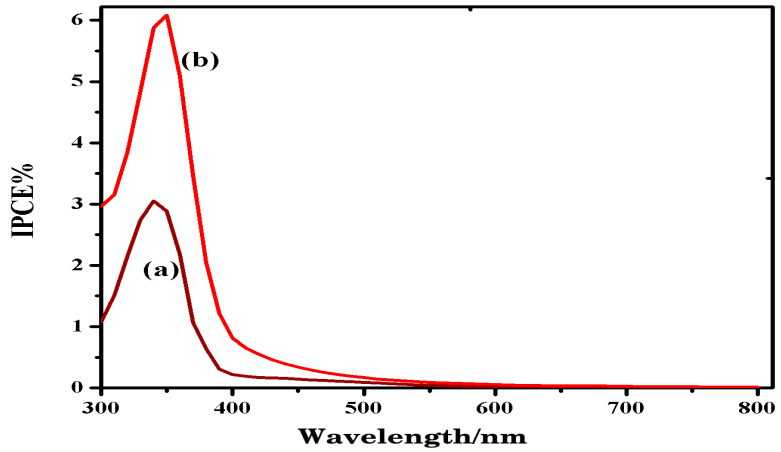

Figure 4.16: IPCE of ZnO based DSSCs sensitized by *Bougainvillea* extracted with a) H_2O b) ethanol.

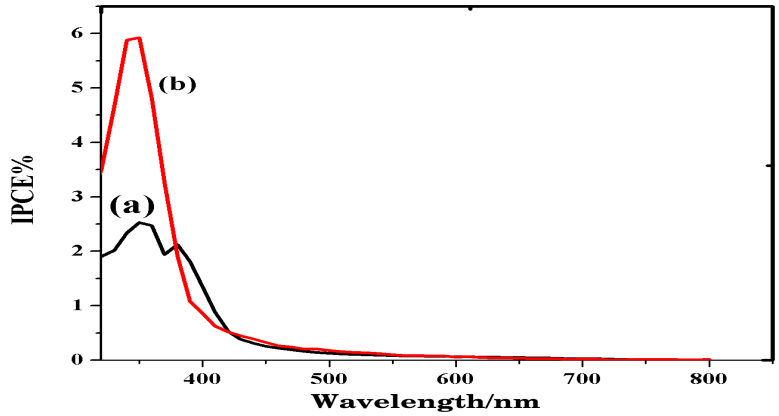

Figure 4.17: IPCE of ZnO based DSSCs sensitized by *carissa* extracted with a) H_2O b) ethanol.

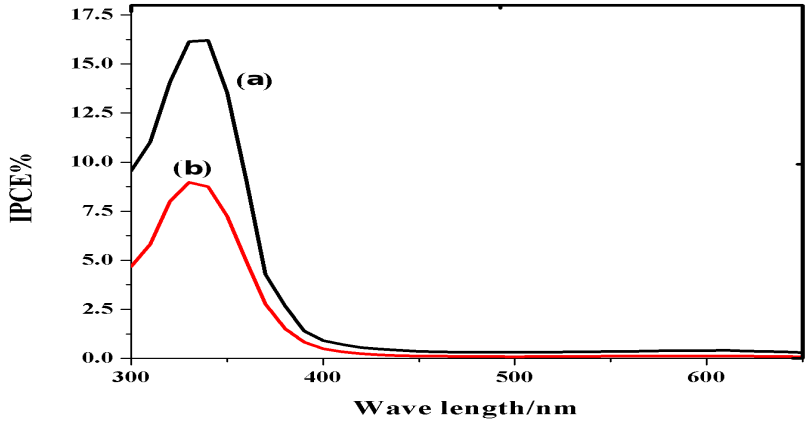

Figure 4.18: IPCE of ZnO based DSSCs sensitized by *Hibiscus* extracted with a) H_2O b) ethanol.

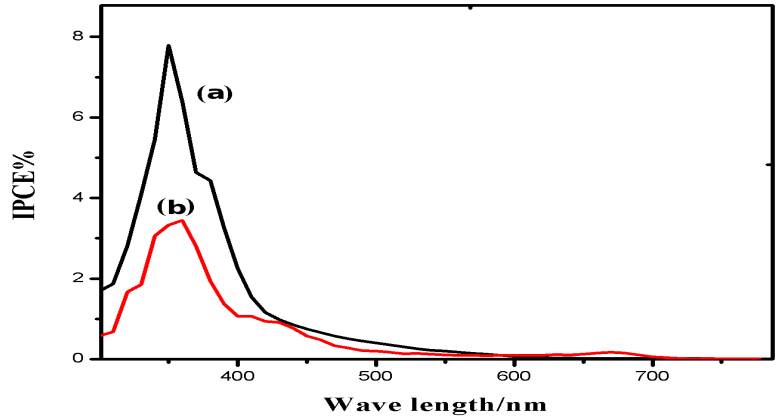

Figure 4.19: IPCE of ZnO based DSSCs sensitized by *Iresine* extracted with a) H_2O b) ethanol.

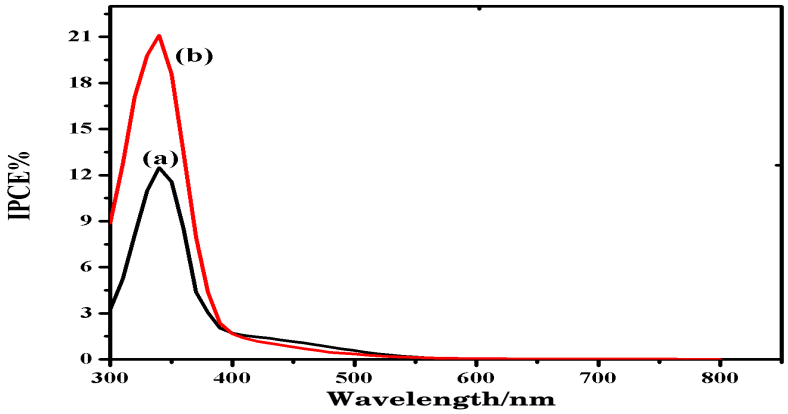

Figure 4.20: IPCE of ZnO based DSSCs sensitized by *Beta vulgaris* extracted with a) H_2O b) ethanol.

Low IPCE results in either inefficient light harvesting efficiency (LHE) by the dye, inefficient charge injection into ZnO, or inefficient collection of injected electrons. A low LHE can be due to a low dye absorption coefficient over the solar spectrum, a low dye concentration, a thin ZnO film to support large concentration of adsorbed dye which absorbs a significant fraction of the incident light, insufficient light scattering within the film, absorption of light by ZnO or the redox electrolyte, and dye degradation [61].

Low η_{inj} can be due to dye desorption, dye aggregation or the excited state levels of the dye lying below the conduction band edge of ZnO, the presence of the surrounding electrolyte, the wavelength of the exciting photon. Low η_{cc} is due to competition between fast recombination of photo-injected electrons with the redox electrolyte or oxidized dye and electron collection.

The formation of Zn^{2+}/dye complex can agglomerate which comes from dissolution of the nanostructured film form a thick covering layer instead of a monolayer, and is therefore inactive for electron injection which also limit the incident photon to current conversion efficiency. In IPCE of H_2O extract of *Carissa ovata*, both H_2O, and ethanol extract of *Amarathus iresine* shows additional spectral peaks which are a quite strong evidence of aggregate formation. The presence of aggregated dyes or non injecting dyes at the surface affect all parameters.

The incident photon-to-current efficiency (IPCE) spectra of ZnO electrodes sensitized with natural dyes and the UV-vis spectra of those sensitizers with there respective maximum wavelength are given in Table 4.2.

Table 4.2: Absorption maxima with photo-action spectra maxima for ZnO based DSSCs.

Sensitizers	Solvent	Absorption(λ_{max})	Photoaction Spectra	
			λ_{max}	IPCE%
Carissa Ovata	Water	553	350	2.5
	Ethanol	536, 664	346	5.9
Jacaranda mimosofolia	Water	——	338	7.6
	Ethanol	536	340	15.2
Beta vulgaris	Water	419, 533	338	12.5
	Ethanol	474	340	21.1
Bougainvillea spectabilis	Water	485, 531	340	3.1
	Ethanol	470, 536, 610, 664	349.5	6.1
Hibiscus sabdariffa	Water	519	338	16.5
	Ethanol	548	329	8.9
Amarathus iresine	Water	532	350	7.8
	Ethanol	413, 433, 464, 664	360	3.4

In all DSSCs device studied a small value of the incident to photon conversion efficiency, short circuit current, and fill factor were obtained that leads to small solar to electricity conversion efficiency.

In view of the instability of ZnO in acidic dyes, the development of new types of photosensitizers for use in ZnO DSSCs is a subject that has already been widely investigated. These photosensitizers are expected to be chemically bonded to the ZnO semiconductor, be charge transferable with a high injection efficiency, and be effective for light absorption in a broad wavelength range. New types of dyes should be developed with the aim of fulfilling these criteria. For our study some of the chlorophyll extract shows relatively good efficiency for ethanol extract than water extract. But to see the effectiveness of the sensitizers we have used for ZnO based DSSCs and to investigate and to check ether the problem comes due to ZnO nanoparticle or other, we performed and characterized the

well known TiO_2 nanoparticle based solar cell with some of the sensitizers which are used for sensitizing ZnO nanoparticle.

For the three sensitizers the J-V curve have showed a good rectification which also results good photoelectrochemical performances. For *Bougainvillea spectabilis* and *Jacaranda mimosofolia* sensitizers extracted by ethanol, in both case the current density is relatively maximum than water extract which is due to the fast injection of electron. But the V_{oc} is good for water extract whch mean that the recombination to oxidized dye or to oxidized electrolyte is poor.

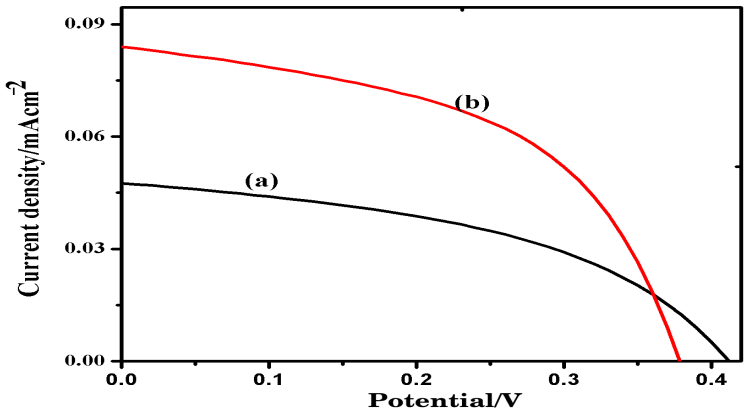

Figure 4.21: J-V of TiO_2 based DSSCs sensitized by a) Water b) Ethanol extract of *Bougainvillea spectabilis* .

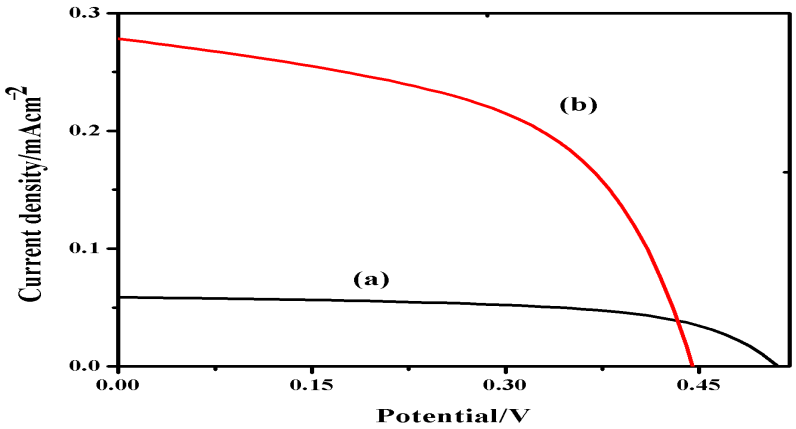

Figure 4.22: J-V of TiO_2 sensitized by a) Water b) Ethanol extract of *Jacaranda mimosofolia*.

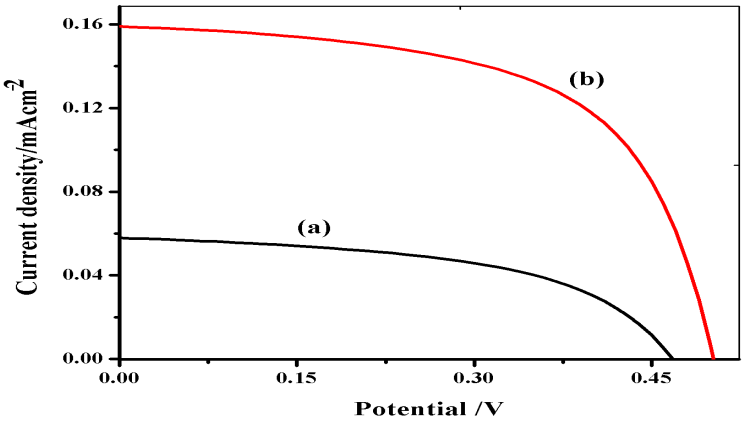

Figure 4.23: J-V of TiO_2 based DSSCs sensitized by a) Water b) Ethanol extract of *Carissa ovata*.

The IPCE Spectrum of this sensitizers showed that, there is a good sensitization of the TiO_2 nanoparticle to the visible spectrum which is responsible for the increment of the photoelectrochemical performance for this sensitizers. The IPCE onset of the device from ethanol extract dye starts at the longest wavelength as compared to water extract. And from this result we conclude that the sensitizers we have used for TiO_2 as well as for the ZnO have the ability to sensitize the nanoparticle to absorb in the visible region but the semiconductor nature made the difference.

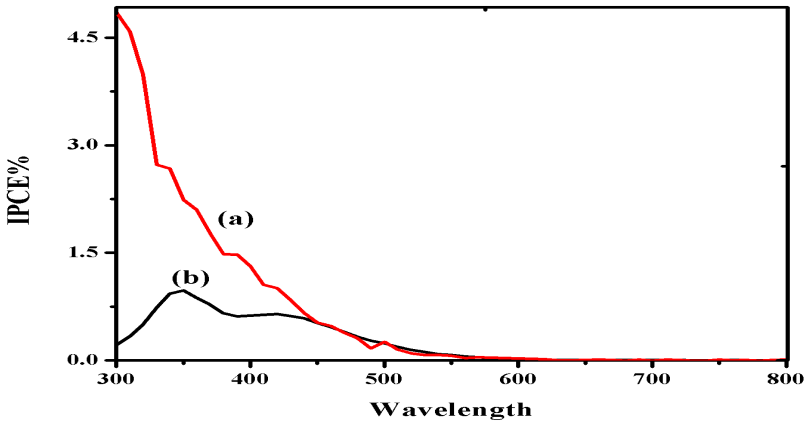

Figure 4.24: IPCE of TiO_2 based DSSCs sensitized by a) Water b) Ethanol extract of *Bougainvillea spectabilis*.

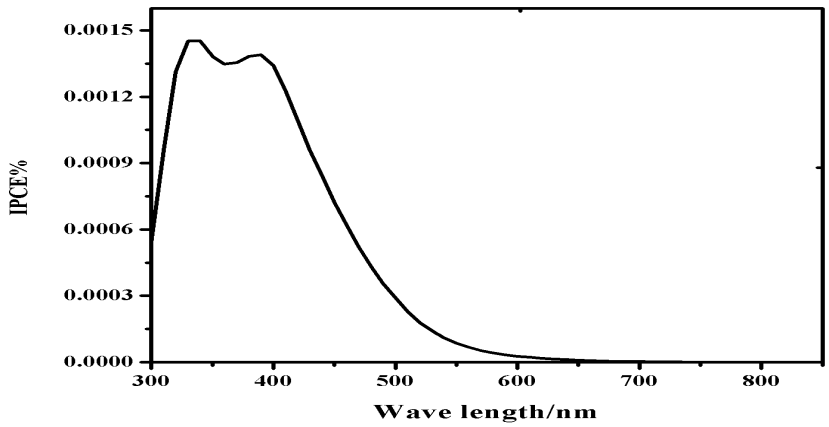

Figure 4.25: IPCE of TiO_2 based DSSCs sensitized by Ethanol extract of *Jacaranda mimosofolia* .

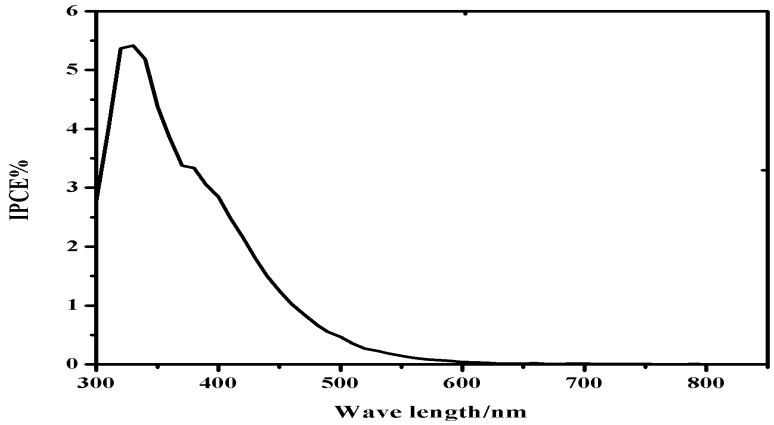

Figure 4.26: IPCE of TiO_2 based DSSCs sensitized by Water extract of *Jacaranda mimosofolia*.

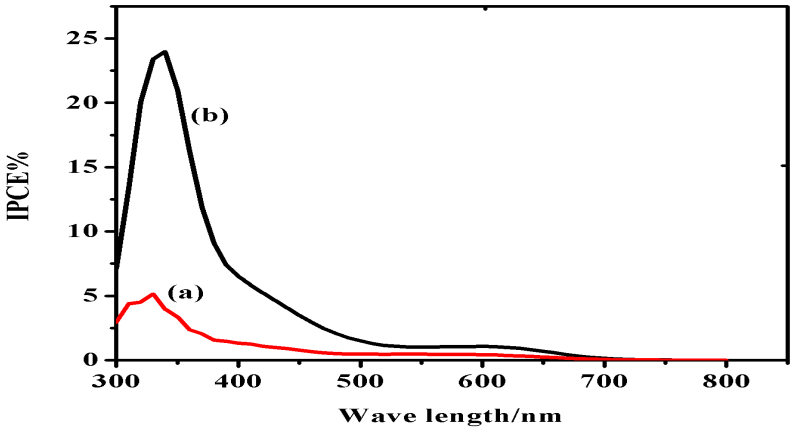

Figure 4.27: IPCE of TiO_2 based DSSCs sensitized by a) Water b) ethanol extract of *Carissa ovata*.

The performance of the DSSCs based on TiO_2 in terms of short-circuit photo-current (J_{sc}), open-circuit voltage (V_{oc}), fill factor (FF), and energy conversion efficiency (η) of *Bougainvillea spectabilis, Carissa ovata,* and *Jacaranda mimosifolia* which are extracted using the same solvent Ethanol and water are shown in Table 4.3.

Table 4.3: Photovoltaic performance of DSSCs based on TiO_2 nanoparticles with different sensitizers

Natural Sensitizers	Extracting Solvent	J_{Sc}	V_{oc}	FF%	η
Bougainvillea spectabilis	Ethanol	0.084	0.38	50.7	0.016
	Water	0.047	0.48	44.3	0.009
Carissa ovata	Ethanol	0.159	0.51	58.6	0.047
	Water	0.058	0.47	44.8	0.012
Jacaranda mimosifolia	Ethanol	0.17	0.45	52.3	0.041
	Water	0.059	0.52	58.5	0.018

The incident photon to current conversion efficiency (IPCE) spectra of TiO_2 electrodes sensitized with the above three natural dyes and the UV-vis spectra of those sensitizers with their respective maximum wavelength are shown in Table 4.4.

Table 4.4: Absorption with photo-action spectra maxima for TiO_2 based DSSCs.

Sensitizers	Solvent	Absorption (λ_{max})	Photo action spectra	
			λ_{max}	IPCE
Bougainvillea spectabilis	Ethanol	536, 610, 664	348, 419	0.96, 0.6
	Water	485, 531	390, 419	2.7, 1.03
Carissa ovata	Ethanol	536, 664	595	23.8, 1.08
	Water	553	330, 540	5.11, 0.47
Jacaranda mimosofolia	Ethanol	536	390	0.0014
	Water	——	327, 381	3.36

TiO_2 based solar cells give higher power conversion efficiencies than the correspond ing

ZnO based solar cells sensitized by the same sensitizers. It gives higher photocurrents, open circuit voltage, and fill factors. The overall conversion efficiency was also found to be rather low for ZnO based cell for all cells sensitized by the same natural dye. This is because TiO_2 semiconductor nanoparticle the extracted natural dyes can attach easily using it's hydroxyl or carboxyl group with the porous semiconductor. The other reason may be due to a higher electron injection efficiency from excited dye molecules into the TiO_2 conduction band and/or a higher dye regeneration efficiency, which are responsible for increment of the performance of this cell, than that of ZnO based solar cell.

In this study the the TiO_2 based solar cell was characterized only to check to which extent, our natural dye sensitized ZnO based DSSCs perform with respect to the commercial TiO_2 nanoparticle based DSSCs. It was known that a small concentration of acids are important for extraction of natural pigments which are good for sensitization of nanoparticle electrodes, but in our case acids are not good for ZnO because of the amphoteric behavior the oxide. Due to this our work shows that it is also possible to use water and ethanol for extraction of natural pigments, and to use those pigment for sensitization of ZnO nanoparticle.

In water extract of natural dye, increased socking time of the film will leads to the dissolution of ZnO nanopartricle on the ITO, this is because of the extraction solvent (water) possesses an acidic nature, protons derived from dissolution of the dye makes the dye solution relatively acidic and this may be one of the reason for decrease in the short-circuit photocurrent. Also upon long socking time, formation of aggregate are formed which can be center of charge recombination and decrease the photovoltaic effects.

Generally, natural dyes suffer from low V_{oc}, J_{sc} which leads lower power conversion efficiency than an equivalent commercial N719 sensitized cell. This is because of most of natural dyes didn't completely attached to the ZnO nanopartciles, even upon washing by solvent to avoid aggregation from the socked film, the sensitizers leave the surface of the film, this is due to, more of the natural dye attached with film of the nanoparticles by physical attaching or by a weak bonding force.

Chapter 5

Conclusion

In this work, we have successfully synthesize ZnO nanoparticles which is one of the major semicondcutor for DSSCs, using polyethylene glycol as despersing agent. The average particle size of these semiconductor nanoparticles were determined using an approximation model called the effective mass model. From optical absorption spectra the maximum absorption λ_{max} was determined which were used for finding the energy band gap of the nanoparticles. From the effective mass approximation which relates the radius of nanoparticle with its energy bandgap we determined the size of ZnO nanoparticle to be 1.14 nm.

Natural dyes were extracted form six different sensitizers using water and ethanol as a solvent. These dyes were used to sensitize ZnO nanoparticle to absorb in the visible region of spectrum. The sensitization process were analyzed by comparing the IPCE of the device, the absorption spectrum of the solution and zinc oxide nanoparticles.

DSSCs device are fabricated using ZnO nanoparticles for all the six sensitizers and their photovolatic performance were determined. For ethanol extract of *Jacaranda mimosifolia, Bougainvillea spectabilis, Carissa ovata, Amarathus iresine, Beta vulgaris, and Hibiscus sabdariffa*, efficiency of 0.0063, 0.0066, 0.0031, 0.039, 0.0039, 0.0043, respectively were obtained. For water extract of *Jacaranda mimosifolia, Bougainvillea spectabilis, Carissa ovata, Amarathus iresine, Beta vulgaris*, and *Hibiscus sabdariffa* we have reached an efficiency of 0.002, 0.0016, 0.003, 0.0062, 0.0077, 0.0104, respectively were obtained.

For comparative study commercial TiO_2 nanoparticle were used, and the device using some of the natural dye sensitizers (*Jacaranda mimosifolia, Bougainvillea spectabilis, Carissa ovata* was constructed and characterized. For these three sensitizers using TiO_2 nanoparticle with ethanol extract efficiency of 0.041, 0.016, 0.047 respectively were obtained. For water extract efficiency of 0.018, 0.012, 0.009 respectively were obtained.

In general ZnO nanopartcles based DSSCs shows low photoelectrochemical performance as compared to commercial TiO_2 based DSSCs sensitized with the same sensitizers. Some of the limiting factor for this were, insufficient attachment of natural dyes with the nanoparticles, formation of aggregation between the nanoparticles up on film formation, low injection, low regeneration of electron, formation of Zn^{2+}/dye complex. Generally DSSCs based on ZnO nanopartcles were one of the research area in which most of researchers focused on improving stability by making different modification. The modification of ZnO aggregates with a very effective shell material on ZnO, preventing the generation of Zn^{2+}/dye agglomerates will be a good method for improving the stability of ZnO nanopartcles.

Bibliography

[1] M. Grätzel. *Nature*, 414:338, 2001.

[2] A. E. Becquerel. *Cent. Aca. sci. par.*, 9:561, 1839.

[3] W. Smith. *Nature*, 7:303, 1873.

[4] W. G. Adams and R. E. Day. *Proc. R. Soc. Lond.*, 125:113, 1877.

[5] W. West. *Photogr. Sci. Eng.*, 18:35, 1974.

[6] A. B. Ellis, S. W. Kaiser, and M. S. Wrighton. *J. Am. Chem. Soc.*, 98:1635, 1976.

[7] Di Wei and Gehan Amaratunga. *Int. J. Electrochem.*, 2:897, 2007.

[8] B. O'Regan and M. Graetzel. *Nature*, 353:737, 1991.

[9] H. Tsubomura, M. Matsumura, Y. Nomunara, and T. Amamiya. *Nature*, 261:402, 1976.

[10] R. Katoh, A. Furube, T. Yoshihara, K. Hata, G. Fujihashi, S. Takano, S. Murata, H. Arakawa, and M. Tachiya. *J. Photochem*, 108:4818, 2004.

[11] C. Bauer, G. Boschloo, E. Mukhtar, and A. Hagfeldt. *J. Phys. Chem.*, 105:5585, 2001.

[12] L. Forro, O. Chauvet, D. Emin, L. Zuppiroli, and H. Berger F. Levy. *J. Appl. Phys.*, 75:633, 1994.

[13] L. Schmidt-Mende and J. L. MacManus-Driscoll. *Mate. Today*, 10:40, 2007.

[14] M. Saito and S. Fujihara. *Ener. Envir. Sci.*, 1:280, 2008.

[15] Y. Chiba, A. Islam Y. Watanabe, R. Komiya, N. Koide, and L. Y. Han. *Japan. J. Appl. Phy.*, 45:638, 2006.

[16] J. Portier, H.S. Hilal, I. Saadeddin, S. J. Hwang, M.A. Subramanian, and G. Campet. *Prog. Sol. Sta. Chem*, 32:207, 2004.

[17] M. K. I. Senevirathne, P. K. D. D. P. Pitigala, V. Sivakumar, P.V.V.Jayaweera, A.G.U. Perera, and K. Tennakone. *J. Photochem. Photobiol.*, 195:364, 2008.

[18] R. A. Laudise and A. A. Ballman. *J. Phys. Chem.*, 64:688, 1960.

[19] L. N. Demianets, D. V. Kostomarov, I. P. Kuzmina, and S. V.Pushko. *Crystallogr. Rep.*, 47:586, 2002.

[20] B. Liu and H. C. Zeng. *Langmuir*, 20:4196, 2004.

[21] R. Viswanatha, H. Amenitsch, and D. D. Sarmakinetics. *J. Am. Chem. Soc.*, 129:4470, 2007.

[22] J. Zhang, L. D. Sun, J. L. Yin, H. L. Su, C. S.L iao, and C. H. Yan. *Chem. Mater.*, 14:4172, 2002.

[23] A. Kawska, P. Duchstein, O.Hochrein, and D.Zahn. *Nano Lett.*, 8:2336, 2008.

[24] H. L. Cao, X. F. Qian, Q. Gong, W. M. Du, X. D. Ma, and Z. K. Zhu. *Nanotech.*, 17:3632, 2006.

[25] Y. h. Zhang Y. C. Zhai and X. Y. Shen. *Trans. Nonferrous Met. Soc.*, 20:236, 2010.

[26] N. S. Pesika, K. J. Stebe, and P. C. Searson. *J. Phys. Chem.*, 107:10412, 2003.

[27] N. H. Quang, N. T. Truc, and Y. M. Niquet. *Comp. Mater. Sci.*, 44:21, 2008.

[28] J. Singh. *J. NonCry. Soli.*, 299:444, 2002.

[29] M. K. Nazeeruddin, A. Kay, I. Rodicio, R. Humphry-Baker, E. Müller, P. Liska, N. Vlacho-poulos, and M. Grätzel. *J. Am. Chem. Soc.*, 115:193, 1993.

[30] M. S. Roy, P. Balraju, M. Kumar, and G. D. Sharma. *Sol. Ener. Mat.*, 92:909, 2008.

[31] G. Zhang, H. Bala, Y. Cheng, D. Shi, X. Lv, Q. Yu, and P. Wang. *Chem. Commun.*, 23:2198, 2009.

[32] M. Striccoli, P. Cosma, and A.Agostiano. *Bio. Electrochem.*, 33:59, 2005.

[33] H. Kim, N. Dashdorj, H. Zhang, J. Yan, W. A. Cramer, and S. Savikhin. *Biophys. J.*, 89:567, 2005.

[34] A. Petrella, P. D. Cozzoli, M. L. Curri, M. Striccoli, P. Cosma, and A. Agostiano. *Bioele. chem.*, 63:99, 2004.

[35] J. Sullivan. *Newsletter*, 27:86, 1998.

[36] T. Goto and T. Kondo. *Angew. Chem. Int. Ed. Engl*, 30:17, 1991.

[37] F. J. Heredia, E. M. Francia-Aricha, J. C. Rivas-Gonzalo, I. M. Vicario, and C. Santos-Buelga. *food chem.*, 63:491, 1998.

[38] J. B. Harborne. *Biochem. J.*, 7:22, 1958.

[39] A. Zyoud. *Nanoparticle CdS-Sensitized TiO_2 Catalyst for Photo degradation of Water Organic Contaminants*. PhD thesis, An-Najah National University, Palestine, 2009.

[40] G. Calogero, a G. Di Marco, S. Caramori, S. Cazzanti, R. Argazzic, and C. A. Bignozzi. *Energy Environ. Sci*, 2:1162, 2009.

[41] M. A. Green, K. Emery, Y. Hishikawa, W. Warta, and E. D. Dunlop. *Prog. Photovol.*, 19:565, 2011.

[42] G. Boschloo and A.Hagfeldt. *Acc. Chem. Res*, 42:1819, 2009.

[43] P. Wang, S. M. Zakeeruddin, J. E. Moser, T. Sekiguchi, and M. Grätzel. *Nature. Mater.*, 2:402, 2003.

[44] A. F. Nogueira, C. Longo, and M. A. De Paoli. Coord. *Chem. Rev*, 248:248, 2004.

[45] C. H. Yoon, R. Vittal, J. Lee, W. S. Chae, and K. J. Kim. *Electrochim. Acta*, 53:2890, 2008.

[46] T. N. Murakami and M. Grätzel. *Inorg. Chim. Acta*, 361:572, 2008.

[47] T. H. Tsai, T. W. Chen, S. M. Chen, and K. C. Lin. *Int. J. Electrochem. Sci.*, 6:2058, 2011.

[48] V. S. Vasantha and S. M. Chen. *J. Electroanal. Chem.*, 77:592, 2006.

[49] W. Hong, Y. Xu, G. Lu, C. Li, and G. Shi. *Electrochem. Commun.*, 10:1555, 2008.

[50] J. Nelson. *Imper. Coll. Pres.*, 98:345, 2003.

[51] J. Halme, P. Vahermaa, K. Miettunen, and P. Lund. *Adva. Mate.*, 22:210, 2010.

[52] J. Cai, N. Satoh, and L. Han. *J. Phys.Chem.*, 115:6033, 2011.

[53] J. P. Gònzalez-Vàzquez, J. A. Anta, and J. Bisquert. *J. Phys.Chem.*, 98:5552, 1994.

[54] P. J. Cameron, L.M. Peter, and S. Hore. *J. Phys. Chem.*, 109:930, 2005.

[55] S. Kang, J. Wu, S. Hao, Z. Lan, and J. Lin. *Ener. Sour.*, 32:1568, 2010.

[56] P. Kumbhakar, D. Singh, C. S. Tiwary, and A. K. Mitra. *Chalcogenide Lett.*, 5:387, 2008.

[57] Q. Zhang, C. S. Dandeneau, X. Zhou, and G. Cao. *Adv. Mater.*, 21:4087, 2009.

[58] H. Horiuchi, R. Katoh, K. Hara, S. Murata, and M. Tachiya. *J. Phys. Chem.*, 107:2570, 2003.

[59] K. Keis, C. Bauer, G. Boschloo, A. Hagfeldt, K. Westermark, H. Rensmo, and H. Siegbahn.

[60] C. G., Garcia, A. S. Polo, and N. Y. Iha. *J. Photochem. Photobiol*, 87:160, 2003.

[61] E. Hosono, S. Fujihara, and Kimura. *Electrochi. Acta*, 49:2287, 2004.